Deoxysphingolipids, a novel biomarker for type 2 diabetes, are cytotoxic for insulin-producing cells

Zuellig, Richard A ; Hornemann, Thorsten ; Othman, Alaa ; Hehl, Adrian B ; Bode, Heiko ; Güntert, Tanja ; Ogunshola, Omolara O ; Saponara, Enrica ; Grabliauskaite, Kamile ; Jang, Jae-Hwi ; Ungethuem, Udo ; Wei, Yu ; von Eckardstein, Arnold ; Graf, Rolf ; Sonda, Sabrina

Abstract: Irreversible failure of pancreatic -cells is the main culprit in the pathophysiology of diabetes mellitus, a disease that is now a major global epidemic. Recently, elevated plasma levels of deoxysphingolipids, including 1-deoxysphinganine, have been identified as novel biomarkers for the disease. In this study, we analyzed whether deoxysphingolipids directly compromise the functionality of insulin-producing Ins-1 cells and primary islets. Treatment with 1-deoxysphinganine induced dose-dependent cytotoxicity with senescent, necrotic and apoptotic characteristics and compromised glucose-stimulated insulin secretion. In addition, 1-deoxysphinganine altered cytoskeleton dynamics, resulting in intracellular accumulation of filamentous actin and activation of the RhoGTPase Rac1. Moreover, 1-deoxysphinganine selectively up-regulated ceramide synthase 5 expression and was converted to 1-deoxy-dihydroceramides, without altering normal ceramide levels. Inhibition of intracellular 1-deoxysphinganine trafficking and ceramide synthesis improved the viability of the cells, indicating that the intracellular metabolites of 1-deoxysphinganine contribute to its cytotoxicity. Analyses of signaling pathways identified JNK and p38 MAPK as antagonistic effectors of cellular senescence. Our results revealed that 1-deoxysphinganine is a cytotoxic lipid for insulin-producing cells, suggesting that the increased levels of this sphingolipid observed in diabetic patients may contribute to the reduced functionality of pancreatic -cells. Thus, targeting deoxy-sphingolipid synthesis may complement the currently available therapies of diabetes.

DOI: https://doi.org/10.2337/db13-1042

Deoxysphingolipids, a novel biomarker for type 2 diabetes, are cytotoxic for insulin-producing cells.

Richard A. Zuellig[1#], Thorsten Hornemann[2,3,4#], Alaa Othman[2,3,4], Adrian B. Hehl[5], Heiko Bode[2,3,4], Tanja Güntert[6], Omolara O. Ogunshola[6], Enrica Saponara[7], Kamile Grabliauskaite[7], Jae-Hwi Jang[7], Udo, Ungethuem[7], Yu Wei[2,3,4], Arnold von Eckardstein[2,3,4], Rolf Graf[7] and Sabrina Sonda[7*]

[1]Division of Endocrinology, Diabetes and Clinical Nutrition, University Hospital Zurich, [2]Institute for Clinical Chemistry, University Hospital Zurich, [3]Centre for Integrative Human Physiology, University of Zurich, Zurich, Switzerland, [4]Competence Centre for Systems Physiology and Metabolic Diseases, Zurich, [5] Institute of Parasitology, University of Zurich, [6]Institute of Veterinary Physiology, University of Zurich,[7]Swiss Hepato-Pancreatico-Biliary (HPB)-Center, Division of Surgical Research, Departement of Visceral & Transplantation Surgery, University Hospital Zurich, Switzerland.

# Contributed equally to this work

Running title: Deoxysphingolipids and diabetes

* *Address correspondence to:*

Sabrina Sonda

Pancreatitis Research Laboratory

Department of Visceral and Transplantation Surgery

University Hospital Zurich

Rämistrasse 100, DL36,8091 Zurich, Switzerland

sabrina.sonda@usz.ch

Word count: 3991

Figure and table number: eight figures

Abstract

Irreversible failure of pancreatic β-cells is the main culprit in the pathophysiology of diabetes mellitus, a disease that is now a major global epidemic. Recently, elevated plasma levels of deoxysphingolipids, including 1-deoxysphinganine, have been identified as novel biomarkers for the disease. In this study, we analyzed whether deoxysphingolipids directly compromise the functionality of insulin-producing Ins-1 cells and primary islets. Treatment with 1-deoxysphinganine induced dose-dependent cytotoxicity with senescent, necrotic and apoptotic characteristics and compromised glucose-stimulated insulin secretion. In addition, 1-deoxysphinganine altered cytoskeleton dynamics, resulting in intracellular accumulation of filamentous actin and activation of the RhoGTPase Rac1. Moreover, 1-deoxysphinganine selectively up-regulated ceramide synthase 5 expression and was converted to 1-deoxy-dihydroceramides, without altering normal ceramide levels. Inhibition of intracellular 1-deoxysphinganine trafficking and ceramide synthesis improved the viability of the cells, indicating that the intracellular metabolites of 1-deoxysphinganine contribute to its cytotoxicity. Analyses of signaling pathways identified JNK and p38 MAPK as antagonistic effectors of cellular senescence. Our results revealed that 1-deoxysphinganine is a cytotoxic lipid for insulin-producing cells, suggesting that the increased levels of this sphingolipid observed in diabetic patients may contribute to the reduced functionality of pancreatic β-cells. Thus, targeting deoxy-sphingolipid synthesis may complement the currently available therapies of diabetes.

Introduction

In the last three decades, the prevalence of diabetes has been rising worldwide at a dramatic rate, with incidence projections approaching 8% of the population by 2030 (1; 2). This remarkable increase is largely due to the epidemic spreading of type 2 diabetes mellitus (T2DM), which accounts for 90% of all cases of diabetes mellitus worldwide (reviewed in (3; 4)). Given the level of complexity associated with the pathophysiology of T2DM, understanding the mechanisms underlying this disease is necessary to design alternative strategies to limit its progression. Recently, substantial improvements occurred in the detection of early stage or undiagnosed T2DM, thus allowing appropriate treatments in high risk populations. One of the latest biomarkers identified in patients with diabetes and metabolic syndromes are increased plasma levels of deoxy-sphingolipids (1-deoxySLs) (5; 6), a type of sphingolipid characterized by an initial condensation of alanine or glycine instead of serine with palmitic acid and the resultant absence of the hydroxyl group in position C1. Consequently, although these deoxy-sphingoid bases can be acylated to deoxy-dihydroceramides, they cannot be further metabolized to complex sphingolipids or efficiently degraded by the canonical degradation pathway, and thus tend to accumulate once produced. Importantly, 1-deoxySLs display toxic properties *in vitro* toward several cell lines (7-9) and *in vivo* are thought to impair neuronal functionality in patients with the hereditary sensory and autonomic neuropathy type I (HSAN1) (10).

In light of the increased plasma levels of 1-deoxySLs found in diabetic patients and of the reported cytotoxic effects associated with the exposure to increased 1-deoxySL concentrations, we investigated whether these atypical sphingolipids directly compromise pancreatic β-cells, the dysfunction of which plays an important role in the pathogenesis of both type 1 and type 2 diabetes.

Research Design and Methods

Biochemical reagents

Unless otherwise stated, all chemicals were purchased from Sigma and cell culture reagents from Gibco-BRL. Inhibitor stock solutions were freshly diluted to the concentrations required for the individual experiment indicated in the figure legends. Lipid stock solutions were prepared as a bovine serum albumin (BSA) complex, as described in (10), and added to the cells at the concentrations indicated in the figure legends. BSA was used as control.

In vitro cell culture

The Ins-1 rat insulinoma cell clone 832/13, generously provided by C. Wollheim, was maintained in RPMI 1640 medium, as described (11; 12). Cell metabolic activity was tested with 0.5% tetrazolium salt solution 3-(4,5-dimethylthiazol-2-yl)-2,5-diphenyltetrazolium bromide (MTT), or WST-1 (Roche), according to the manufacturer's instructions. Cell death was quantified by trypan blue exclusion or lactate dehydrogenase (LDH) release in the medium (Roche). Cellular senescence was quantified with the β-galactosidase assay kit (Cell Biolabs). Adp21 (rat) and AdGFP adenovirus were purchased from Vector Biolabs, Philadelphia, USA. Rac1 activity was measured with G-LISA Rac1 activation assay (Cytoskeleton, Denver, USA).

Animal experiments

Wistar rats, leptin deficient ob/ob mice on C57BL/6J background (B6.V-*Lep*/OlaHsd) and wild type (WT) C57BL/6J (Harlan Laboratories) were kept under a light-dark regime (16:8 h), constant temperature, and free access to food and water. All animal experiments were performed

in accordance with swiss federal animal regulations and approved by the cantonal veterinary office of Zurich.

Islets were harvested from pancreata of male Wistar rats (250 to 300 g) by collagenase (NB8 collagenase, Serva, Heidelberg, Germany) followed by trypsin digestion to dissociate them into single cells, according to (13).

Insulin secretion

Dissociated islets cells were seeded in 12-well ECM coated plates (Novamed, Jerusalem, Israel), treated for 24 h with 5 μM sphinganine, 1-deoxysphinganine or BSA and incubated in RPMI medium containing 3.3 mM glucose for 1 h. Following sequential 1 h incubations with low (3.3 mM), high (16.7 mM), low (3.3 mM) glucose concentrations, insulin secretion was measured by radioimmunoassay (Insulin-CT, CIS, Biointernational, Schering AG, Baar, Switzerland), according to the manufacturer's instructions.

qRT-PCR

Total RNA was extracted from Ins-1 cells cultured in 1 μM sphinganine or 1-deoxysphinganine for 24 h. Quality of RNA was assessed by 2100 bioanalyzer (Agilent Technologies, Basel, Switzerland). cDNA was obtained with the RT2 First Strand Kit and profiled using the Rat Cell Death Pathway Finder PCR Array (both from SABiosciences, Hombrechtikon, Switzerland), according to the manufacturer's instructions. CerS primers for SYBR green qPCR are listed in Supplementary Materials and Methods.

Immunohistochemistry and flow cytometry analyses

Pancreas specimens were fixed in 4% formalin and paraffin embedded according to standard procedures (14). Ins-1 cells were fixed in 3.6% formaldehyde and permeabilized with 0.2% Triton X-100 in PBS. Primary antibodies used in this study are listed in Supplementary Materials

and Methods. Apoptosis detection was performed with an ApopTag peroxidase Kit (MP Biomedicals, Illkirch, France). Immunofluorescence analysis and image data collection were performed on a Zeiss Axioplan 2 Imaging fluorescence microscope (Carl Zeiss Microimaging, Göttingen, Germany), or on a Leica SP2 AOBS confocal laser-scanning microscope (Leica Microsystems, Wetzlar, Germany) using a glycerol immersion objective lens (Leica, HCX PL APO CS 63x 1.3 Corr). Image z-stacks were collected with a pinhole setting of Airy 1 and twofold oversampling. Image stacks of optical sections were processed using the Huygens deconvolution software package version 2.7 (Scientific Volume Imaging, Hilversum, NL). Three-dimensional reconstruction, volume rendering, and quantification of signal overlap in the 3D volume model were done with the Imaris software suite (Version 7.2.1, Bitplane, Zurich, Switzerland). The degree of signal overlap in the 3D volume models is shown graphically as scatterplots by plotting the intensity of two fluorescent signals in each voxel of the 3D model. Voxels with similar signal intensity for both signals appear in the area of the diagonal.

Single-cell quantification of stained cells by flow cytometry was performed using a FACSDiva flow cytometer (BD Bioscences, Allschwil, Switzerland).

Western blotting

Ins-1 cells cultured in 1 μM sphinganine, 1-deoxysphinganine or BSA for 24 h were lysed as described (15). Aliquots corresponding to 35 μg of proteins were separated by SDS-PAGE electrophoresis, blotted and probed over night at 4°C. Primary antibodies used in this study are listed in Supplementary Materials and Methods. Immunoreactive bands from at least 3 independent experiments were quantified by densitometry and normalized to β-actin or GAPDH levels.

Analysis of sphingoid bases and ceramides by LC–MS/MS

The sphingoid base profile was analyzed as described earlier (5). Ceramide species were extracted by adding 1 ml methanol/chloroform (2:1) (including 200 pmole of C12 ceramide internal standard (Avanti Polar Lipids) to 100 µl of re-suspended cells followed by the addition of 0.5 ml of chloroform and 200 µl alkaline water (10). Interfering phospholipids were hydrolyzed by re-extracting the dried lipids with methanol-KOH:chloroform (4:1) as described earlier (10). Lipids were separated on a C18 column (Uptispere 120 Å, 5µm, 125 × 2 mm, Interchim, France) and analyzed on a TSQ Quantum Ultra (Thermo, Reinach, Switzerland) using atmospheric pressure chemical ionization (APCI) (10). Ceramides and deoxy-Ceramides were identified by precursor ion scan (20mV collision energy) with fragments of (m/z 264.3) and (m/z 268.3) respectively. Levels were normalized to ISTD and cell numbers.

Statistical analyses

Results are expressed as means ± SEM. Significance was assessed using Student's unpaired, two-tailed *t* tests or one-way analysis of variance. A probability value <0.05 was considered significant. When the overall probability value was <0.05, the Bonferroni multiple-comparison test was used to determine whether there was a significant difference between values of control (reference sample) and samples of interest.

Results

1-deoxySL treatment is cytostatic and cytotoxic for Ins-1 cells

As 1-deoxySLs were found elevated in the plasma of diabetic patients in the low µM range (5; 6), we analyzed whether 1-deoxySLs can directly affect the viability of insulin-secreting cells. To this aim, the rat insulinoma cell line Ins-1 was treated at 50% confluence (Fig. 1A, L: low density) for 24 h with 1-deoxysphinganine or sphinganine as control. 1-deoxysphinganine incubation reduced both the metabolic activity, as measured by MTT (Fig.1A) and WST-1

reduction (Fig. S1A), and the number of live cells (Fig.1B) in a dose-dependent manner. Treatment with 5 μM caused cell round up (Fig. 1C) and death, as shown by robust trypan blue inclusion (Fig.1D) and LDH release (Fig.1E). However, cells treated with 1 μM 1-deoxysphinganine did not increase in number compared with the initial seeding but showed modest levels of lethality (Fig.1D, E), or up-regulation of genes involved in cell death pathways (Fig. S1B-D), suggestive of a cytostatic effect of the lipid at this concentration (Fig. 1B). When the lipid treatment was performed on 90% confluent cells (Fig. 1A, H: high density), the metabolic activity was reduced only at the highest concentration of 1-deoxysphinganine tested, further indicating that 5 μM 1-deoxysphinganine is cytotoxic for both dividing and quiescent cells, while lower lipid concentrations are cytostatic. In addition, treatment for only one hour, followed by washout and subsequent 23 h incubation was sufficient to reduce the metabolic activity of the cells comparably to a continuous 24 h incubation with 1-deoxysphinganine (Fig. 1F), suggesting a rapid effect of the lipid.

1-deoxysphinganine triggers p21-mediated senescence and multiple cell death pathways in Ins-1 cells

We then investigated whether the reduction of replication following low 1-deoxysphinganine concentration is mediated by induction of senescence. 1 μM 1-deoxysphinganine increased β-galactosidase activity (Fig. 2A) and nuclear $p21^{WAF1/Cip1}$ expression (Fig. 2B, C), a hallmark (16) and inducer of senescence (17), respectively. To investigate if increased p21 expression was sufficient to trigger the senescence pathway in Ins-1 cells, we used adenovirus infection overexpressed p21 (Adp21) or GFP (AdGFP) as a control (Fig 2D). Adp21 infection decreased Ins-1 cell replication and increased β-galactosidase activity, while both parameters were unchanged following AdGFP incubation (Fig 2E, F). In addition, the increased β-galactosidase

activity following 1 μM 1-deoxysphinganine treatment or Adp21 infection was accompanied by increased MTT reduction/cell (Fig. S2), suggesting increased mitochondrial dehydrogenase activity, a parameter associated with cellular senescence (18). These data suggest that up-regulation of p21 induced by 1 μM 1-deoxysphinganine treatment contributes to the decreased Ins-1 replication by activating a senescence program.

Next, we further explored the cytotoxic effect of high 1-deoxysphinganine concentrations. Five μM 1-deoxysphinganine abrogated the expression of p21 and induced cells with condensed pyknotic nuclei and high levels of activated caspase-3, hallmarks for the execution phase of apoptosis (Fig. 3A, S3A). In addition, FACS analyses of cells co-stained with annexin V and propidium iodide (PI) revealed that 5 μM 1-deoxysphinganine treatment increased the amount of both apoptotic and necrotic cells (Fig. 3B, C, S3B), and induced the cells to arrest in the G0/G1 phase of the cell cycle (Fig. S4), suggesting that the lipid triggers multiple cell death pathways in Ins-1 cells.

1-deoxysphinganine intracellular metabolites contribute to cytotoxicity in Ins-1 cells

As treatment with exogenous 1-deoxy-dihydroceramides (m18:0,24:1 and m18:0,16:0) and 1-deoxy-methylsphinganine, where alanine is replaced by glycine, reduced the cell replication similarly to 1-deoxysphinganine treatment (Fig. 4A), we then tested whether exogenous 1-deoxysphinganine was also metabolized by the cells to the deoxy forms of ceramide. Incubation with 1-deoxysphinganine significantly increased the cellular levels of deoxy-dihydroceramide with different acyl chain length (Fig. 4B) without altering normal ceramide levels (Fig. S5A), and selectively up-regulated the expression of ceramide synthase 5 (Fig. 4C), suggesting that 1-deoxysphinganine is readily metabolized in Ins-1 cells and accumulates in the acylated form. In addition, pre-treatment of Ins-1 cells with the class 2 amphiphile U-18666A, a well-established

inhibitor of NPC1 (Niemann–Pick C) protein that prevents intracellular trafficking of sphingolipids and cholesterol (19; 20), partially rescued 1-deoxysphinganine-mediated cytotoxicity (Fig. 4D, S5B). Moreover, pharmacological inhibition of ceramide synthesis with fumonisin B1 was unique in reducing the toxicity of 5 μM 1-deoxysphinganine (Fig.4D, S5C), while inhibition of either the first step of sphingolipid synthesis with myriocin or glucosylceramide synthesis with 1-phenyl-2-palmitoylamino-3-morpholino-1-propanol (PPMP) had no effect on cell viability (not shown). Collectively, these data indicate that intracellular uptake followed by metabolic conversion to 1-deoxy-dihydroceramides is responsible, at least in part, for 1-deoxysphinganine toxicity.

1-deoxysphinganine increases the phosphorylation of selected kinases in Ins-1 cells

To further characterize the biochemical components of 1-deoxysphinganine-induced cytotoxicity, we analyzed the phosphorylated status of key proteins involved in major signaling pathways. Western blot quantification revealed increased phosphorylation of JNK and p38 MAPK in 1-deoxysphinganine treated Ins-1 cells. In addition, the ratio of AKT phosphorylation was unchanged upon lipid treatment but the total protein amount increased in presence of 1-deoxysphinganine (Fig. 5A-C). As kinase activation by phosphorylation suggests a possible role of these proteins in 1-deoxysphinganine-mediated phenotype, we tested this hypothesis by treating the cells with specific kinase inhibitors. Pre-treatment with the p38 MAPK inhibitor Birb796 partially rescued cell replication (Fig. 5D) and reduced 1-deoxysphinganine-induced senescence (Fig. 5E). Conversely, the JNK inhibitor SP600125 potentiated cytotoxicity and senescence (Fig. 5D, E), and the combined treatment partially rescued the JNK inhibitor effect at 1 μM 1-deoxysphinganine incubation. These data suggest that p38 MAPK activation is an effector of 1-deoxysphinganine cytotoxicity and senescence, while JNK activation plays a protective role in Ins-1 cells.

1-deoxysphinganine treatment promotes re-organization of the actin cytoskeleton in Ins-1 cells

The observed changes in cell morphology observed following 1-deoxysphinganine treatment (Fig. 1C) prompted us to further analyze whether the lipid induced cytoskeletal alterations. To detect early cytoskeletal re-arrangements, cells were imaged after 5 h of treatment. Phalloidin-stained actin filaments were mainly concentrated in the cortical area and in filopodia following control BSA or sphinganine treatment. However, upon 1-deoxysphinganine incubation, actin staining accumulated in punctated structures mainly located in the peri-nuclear area of the cells. Different from the actin phenotype, tubulin staining showed a similar microtubule pattern in all treatments, suggesting that 1-deoxysphinganine preferentially interferes with the organization of actin cytoskeleton in Ins-1 cells (Fig. 6A). Quantitative analysis of members of the Rho family of GTPases that regulate intracellular actin dynamics (reviewed in (21)), showed increased levels of Rac1 activity (Fig. 6B) and expression of Rac1 and Rho, albeit the latter did not reach significance, upon 1-deoxysphinganine treatment (Fig. 6C), suggesting that Rho family GTPases may be involved in 1-deoxysphinganine-mediated changes in actin cytoskeleton re-organization. Of note, actin alterations were not accompanied by apoptosis at this time point (data not shown). In addition, pre-treatment with JNK, p38 MAPK and ceramide synthase inhibitors did not prevent actin remodeling (Fig. S6A), suggesting that cytoskeletal and cell cycle effects are modulated by different signaling pathways.

To further characterize whether aberrantly localized actin may intersect with the secretory apparatus of the cells, we performed co-staining for actin and insulin. FACS-based single cell quantification revealed that the lipid treatment did not alter the cellular content of actin and insulin (Fig. S6B). However, confocal analyses showed that filamentous actin accumulated

intracellularly in close proximity to and partially co-localized with insulin-containing vesicles (Fig. 6D).

1-deoxysphinganine reduces metabolic activity, insulin secretion and modulates actin cytoskeleton in primary islets

To confirm the relevance of our results in primary cells, we tested whether 1-deoxysphinganine affects the functionality of isolated islets. Lipid delivery to the cells was improved by dissociation of 1400 islets from 6 Wistar rats into single cells, these were seeded in ECM-coated plates and treated for 24 h with 5 μM sphinganine, 1-deoxysphinganine, or BSA as control. Of note, dissociated islets plated on ECM are virtually quiescent (R. Zuellig, personal communication). Under these experimental conditions, 1-deoxysphinganine treatment induced cellular vacuolization (Fig. 7A), and reduced the metabolic activity (Fig. 7B) and, to a lesser extent, the number of live cells (Fig. 7C). However, senescence was not observed, as indicated by comparable βgal activities (Fig. S7A) and absence of p21 staining (not shown). Similarly to the effect in Ins-1 cells, 1-deoxysphinganine treatment induced re-arrangement of actin cytoskeleton with the resulting accumulation of actin in intracellular punctated structures (Fig. 7D). 1-deoxysphinganine did not alter the cellular content of insulin (Fig. S7B) or selectively reduce the number of insulin-producing cells (Fig. S7C). However, following incubation with the lipid, isolated β cells were unable to regulate insulin secretion in response to glucose stimulation (Fig. 7E, S7D). Collectively, these data indicate that 1-deoxysphinganine is cytotoxic to isolated primary islets and compromises both functionality and cyto-architecture of β cells.

Increased glucose levels potentiate 1-deoxysphinganine toxicity

Our *in vitro* results showed 1-deoxySL-mediated cytotoxicity in insulin-producing cells, suggesting that raised levels of these lipids may contribute to the failure of β-cells during the

development of diabetes. However, elevated 1-deoxySLs levels were also found in the plasma of patients with metabolic syndrome that did not present hyperglycemia and overt diabetes (5), raising the question that increased amount of 1-deoxySLs are not the sole cause of β-cell toxicity and that additional factors contribute to the diabetic phenotype. To further investigate the causal network of atypical sphingolipids and β-cell toxicity, we analyzed pancreatic islets in leptin deficient ob/ob mice. Kept on a normal chow diet, these mice develop obesity and a mild hyperglycemia that reverts with aging, as pancreatic β-cell compensation occurs and increased insulin levels improve glucose homeostasis (22; 23). 60 week old ob/ob mice had only slightly higher plasma glucose levels compared with age matched WT animals, but a robust increase in plasma HDL, cholesterol and ALT levels (Fig. S8A), the latter reflecting steatotic liver damage (Fig. S8B). As previously shown (23), ob/ob pancreata were characterized by pronounced islet hyperplasia, vascularization and robust insulin production (Fig. S8B), suggesting that β-cells could compensate for the increased insulin demand without reaching exhaustion. Despite the evident hyperplasia, islets did not show active replication at the analyzed age (Fig. S8B). Interestingly, quantification of the plasma lipid profiles in ob/ob mice revealed a moderate but significant increase of 1-deoxysphinganine levels (Fig. 8A), which was not associated with increased senescence or apoptosis (Fig. S8B). In addition, like in human samples (5), sphingosine was the most abundant species in the mouse plasma and significantly increased in ob/ob mice (Fig. S8C). While it is likely that plasma 1-deoxySLs did not reach a critical concentration threshold to induce β-cell failure, absence of other pathological parameters, including hyperglycemia, may account for the normal viability of β-cells. To test this hypothesis, we incubated Ins-1 cells with 1-deoxysphinganine in presence or absence of glucose. Treatment with 30mM glucose for 24 h potentiated 1-deoxysphinganine-induced toxicity (Fig. 8B, S8D),

suggesting that hyperglycemia and 1-deoxySLs synergize to induce glucolipotoxicity in insulin-producing cells.

Discussion

Elevated levels of 1-deoxySLs have been found in the blood of patients suffering from metabolic syndrome and diabetes mellitus (5; 6), raising the question of the role of atypical lipids in the development of these pathologies. Our results showed that exposure to 1-deoxySLs in the low μM range compromised insulin secretion and triggered senescence and cell death in insulin-producing cells, indicating that 1-deoxySLs are indeed toxic for these cells. In our experimental approach we elucidated 1-deoxysphinganine toxicity at three distinct levels, namely i) changes in cellular structure, ii) engagement of signaling molecules and iii) activation of effector proteins. A major finding of our study is that 1-deoxysphinganine-mediated toxicity is a complex phenomenon and triggers multiple pathways, including cytoskeletal remodeling, senescence, necrosis and apoptosis.

1-deoxysphinganine triggers the re-organization of actin cytoskeleton in insulin-producing cells

1-deoxysphinganine treatment selectively altered cytoskeleton organization both in Ins-1 cells and primary islets, inducing accumulation of filamentous actin in intracellular punctated structures juxtaposed to insulin-containing vesicles. Similar but transient actin fiber alterations have been observed previously in 1-deoxysphinganine-treated Vero cells (7). In addition, 1-deoxysphinganine impaired cytoskeleton dynamics in sensory and motoneurons without inducing cell death (10). Our study showed not only that the lipid induced actin rearrangements before the appearance of apoptotic markers, but also that inhibitors shown to mitigate cytotoxicity did not prevent cytoskeletal remodeling. These data suggest that cytoskeleton rearrangements are a direct effect of 1-deoxysphinganine incubation rather than a consequence of cell lethality and that

cytoskeleton and cell cycle effects are regulated by distinct signaling pathways. In this context, it is currently under investigation whether alterations in Rho GTPase activation, reported by (7) and our study, are the key conserved molecular mechanism also behind cytoskeletal alteration in neurons.

In the case of β-cells, the early cellular morphological alterations may impair cellular functionality, including insulin secretion. Indeed, earlier studies demonstrated that insulin secretion in pancreatic β-cells is coupled with re-organization of the filamentous actin web located beneath the plasma membrane, thus allowing docking of insulin-containing granules to the cell membrane and consequent secretion. Importantly, glucose stimulation directly induces re-arrangement of the actin web (24; 25), to which insulin-containing granules are in tight contact (26). Thus impaired remodeling of actin cytoskeleton resulting from 1-deoxysphinganine treatment may contribute to the defective insulin secretion observed in our primary β-cells cultures. However, we cannot exclude that additional lipid-induced changes, including altered gene transcription, may contribute to the phenotype.

1-deoxy-dihydroceramide contributes to 1-deoxysphinganine-induced cytotoxicity

Ceramide is a key intracellular signaling molecule involved in several cellular functions, including cell death (reviewed in (27)). Importantly, both cell-permeant analogues of ceramide (28) and *de novo* ceramide synthesis (29) impair insulin secretion and mitogenesis in pancreatic *β*-cells and induce apoptosis (reviewed in (30)), supporting a critical regulatory role for ceramide in the metabolic dysfunction of these cells. In the search for the molecular signaling generated by 1-deoxysphinganine treatment, we explored the hypothesis that 1-deoxysphinganine uptake and conversion to 1-deoxy-dihydroceramide is necessary to exert its toxicity. Our mass spectrometry and inhibitor analyses supported this hypothesis. In addition, 1-deoxysphinganine increased the expression of ceramide synthase 5 (CerS5), while β-cell lipotoxicity resulting from palmitate

treatment stimulated the synthesis of CerS4 (31), suggesting that different lipids stimulate specific CerS isoforms. Collectively, our results suggest that some of the cytotoxic effects of 1-deoxysphinganine occur after its intracellular uptake and metabolism to 1-deoxy-dihydroceramide. However, we cannot exclude that 1-deoxysphinganine triggers death receptors on the cell surface. Given the similarity of the molecular structure of 1-deoxysphinganine and sphingosine, it is worthy of further investigation to determine if 1-deoxysphinganine can engage or antagonize the same membrane receptors, as previously suggested (8).

1-deoxysphinganine activates multiple intracellular pathways

In addition to cytoskeletal remodeling, 1-deoxysphinganine treatment induced a complex dose-dependent pattern of toxicity in Ins-1 cells, characterized by the appearance of p21-induced senescence at low doses and apoptosis and necrosis at high doses. Of note, the senescence growth arrest was limited to replicating cells, as demonstrated previously (32-34), and quiescent primary islets were devoid of senescence markers upon lipid treatment. These data imply that 1-deoxysphinganine triggers multiple signaling pathways. Indeed, the lipid was shown to selectively activate JNK, MAPK, Erk1/2, PKC but not AKT in NIH-3T3, RH-7777, PC-3 and LNCaP cell lines (8; 9), while we showed that JNK, p38 MAPK phosphorylation and AKT levels increased in Ins-1 cells, indicating that the intracellular signaling effectors stimulated by 1-deoxysphinganine depend on the cellular context. As JNK and MAPK are known to be activated by intracellular ceramide (35), it is possible that the increased 1-deoxy-dihydroceramide synthesis observed in Ins-1 cells activates these kinases. In addition, the fact that the CerS inhibitor FB1 was the only compound able to rescue the toxicity of high 1-deoxysphinganine doses, suggests that increased ceramide (or its deoxy form) synthesis is upstream of or a prerequisite for the activation of different signaling effectors.

While a more in depth analysis of the set of kinases activated by 1-deoxysphinganine is needed to elucidate the precise downstream signaling cascade, our inhibitor studies revealed an intriguing antagonistic role of JNK and p38 MAPK in the context of 1-deoxysphinganine-induced senescence. Interestingly, a similar dose-dependent senescence-apoptosis transition and opposite effect of p38 MAPK and JNK on senescence has been reported in endothelial progenitor cells upon doxorubicin treatment (36), further confirming that different kinases activated by the same stimulus may exert opposite cellular effects.

In conclusion, our work shows that 1-deoxysphinganine treatment and its conversion to 1-deoxy-dihydroceramide compromises the viability of insulin-producing cells via multiple pathways. This indicates that, similar to free fatty acids (reviewed in (30)), 1-deoxySLs induce lipotoxicity but with higher efficiency (low μM for 1-deoxySLs versus low mM for free fatty acids (31; 37; 38)). However, our *in vivo* study, together with the fact that HSAN1 and metabolic syndrome patients have elevated 1-deoxysphinganine levels without overt diabetes, suggests that the raised amount of 1-deoxysphinganine observed *in vivo* is not sufficient to directly induce β-cell failure but would require additional pathological parameters, for instance an established chronic hyperglycemic state, to promote β-cell toxicity (39). In this context, targeting 1-deoxySL synthesis as a combination therapeutic strategy for diabetes mellitus warrants further investigations.

Acknowledgments

We thank Heidi Seiler for excellent technical assistance and Amedeo Caflisch for providing the Birb796 inhibitor. This research was supported by the Zurich Center for Integrative Human Physiology (ZIHP) and Rare Disease Initiative Zurich (radiz), Clinical Research Priority Program

for Rare Diseases, University of Zurich. No potential conflicts of interest relevant to this article were reported. All the authors of this manuscript contributed in the study design, acquisition, analysis, interpretation of data, drafting and critical revision of the manuscript. R.A.Z., T.H., A.O., A.B.H., E.S., K. G., H.B., Y.W., T.G., O.O.O., J-H.J., U.U. researched data and reviewed/edited manuscript, A.v.E., R.G. contributed to discussion, reviewed/edited manuscript. S.S. wrote manuscript, researched data. S.S. is the guarantor of this work and, as such, had full access to all the data in the study and takes responsibility for the integrity of the data and the accuracy of the data analysis.

References

1. Chen L, Magliano DJ, Zimmet PZ: The worldwide epidemiology of type 2 diabetes mellitus--present and future perspectives. *Nat Rev Endocrinol* 8:228-236, 2012
2. Ashcroft FM, Rorsman P: Diabetes mellitus and the beta cell: the last ten years. *Cell* 148:1160-1171, 2012
3. Prentki M, Nolan CJ: Islet beta cell failure in type 2 diabetes. *J Clin Invest* 116:1802-1812, 2006
4. Donath MY, Ehses JA, Maedler K, Schumann DM, Ellingsgaard H, Eppler E, Reinecke M: Mechanisms of beta-cell death in type 2 diabetes. *Diabetes* 54 Suppl 2:S108-113, 2005
5. Othman A, Rutti MF, Ernst D, Saely CH, Rein P, Drexel H, Porretta-Serapiglia C, Lauria G, Bianchi R, von Eckardstein A, Hornemann T: Plasma deoxysphingolipids: a novel class of biomarkers for the metabolic syndrome? *Diabetologia* 55:421-431, 2012
6. Bertea M, Rutti MF, Othman A, Marti-Jaun J, Hersberger M, von Eckardstein A, Hornemann T: Deoxysphingoid bases as plasma markers in diabetes mellitus. *Lipids Health Dis* 9:84, 2010
7. Cuadros R, Montejo de Garcini E, Wandosell F, Faircloth G, Fernandez-Sousa JM, Avila J: The marine compound spisulosine, an inhibitor of cell proliferation, promotes the disassembly of actin stress fibers. *Cancer Lett* 152:23-29, 2000
8. Salcedo M, Cuevas C, Alonso JL, Otero G, Faircloth G, Fernandez-Sousa JM, Avila J, Wandosell F: The marine sphingolipid-derived compound ES 285 triggers an atypical cell death pathway. *Apoptosis* 12:395-409, 2007
9. Sanchez AM, Malagarie-Cazenave S, Olea N, Vara D, Cuevas C, Diaz-Laviada I: Spisulosine (ES-285) induces prostate tumor PC-3 and LNCaP cell death by de novo synthesis of ceramide and PKCzeta activation. *Eur J Pharmacol* 584:237-245, 2008
10. Penno A, Reilly MM, Houlden H, Laura M, Rentsch K, Niederkofler V, Stoeckli ET, Nicholson G, Eichler F, Brown RH, Jr., von Eckardstein A, Hornemann T: Hereditary sensory neuropathy type 1 is caused by the accumulation of two neurotoxic sphingolipids. *J Biol Chem* 285:11178-11187, 2010
11. Asfari M, Janjic D, Meda P, Li G, Halban PA, Wollheim CB: Establishment of 2-mercaptoethanol-dependent differentiated insulin-secreting cell lines. *Endocrinology* 130:167-178, 1992
12. Hohmeier HE, Mulder H, Chen G, Henkel-Rieger R, Prentki M, Newgard CB: Isolation of INS-1-derived cell lines with robust ATP-sensitive K+ channel-dependent and -independent glucose-stimulated insulin secretion. *Diabetes* 49:424-430, 2000

13. Cavallari G, Zuellig RA, Lehmann R, Weber M, Moritz W: Rat pancreatic islet size standardization by the "hanging drop" technique. *Transplant Proc* 39:2018-2020, 2007
14. Silva A, Weber A, Bain M, Reding T, Heikenwalder M, Sonda S, Graf R: COX-2 is not required for the development of murine chronic pancreatitis. *Am J Physiol Gastrointest Liver Physiol* 300:G968-975, 2011
15. Antoniou X, Gassmann M, Ogunshola OO: Cdk5 interacts with Hif-1alpha in neurons: a new hypoxic signalling mechanism? *Brain Res* 1381:1-10, 2011
16. Rodier F, Campisi J: Four faces of cellular senescence. *J Cell Biol* 192:547-556, 2011
17. Romanov VS, Pospelov VA, Pospelova TV: Cyclin-dependent kinase inhibitor p21(Waf1): contemporary view on its role in senescence and oncogenesis. *Biochemistry (Mosc)* 77:575-584, 2012
18. Kaplon J, Zheng L, Meissl K, Chaneton B, Selivanov VA, Mackay G, van der Burg SH, Verdegaal EM, Cascante M, Shlomi T, Gottlieb E, Peeper DS: A key role for mitochondrial gatekeeper pyruvate dehydrogenase in oncogene-induced senescence. *Nature* 498:109-112, 2013
19. Lloyd-Evans E, Platt FM: Lipids on trial: the search for the offending metabolite in Niemann-Pick type C disease. *Traffic* 11:419-428, 2010
20. Ikonen E, Holtta-Vuori M: Cellular pathology of Niemann-Pick type C disease. *Semin Cell Dev Biol* 15:445-454, 2004
21. Heasman SJ, Ridley AJ: Mammalian Rho GTPases: new insights into their functions from in vivo studies. *Nat Rev Mol Cell Biol* 9:690-701, 2008
22. Genuth SM, Przybylski RJ, Rosenberg DM: Insulin resistance in genetically obese, hyperglycemic mice. *Endocrinology* 88:1230-1238, 1971
23. Hoppener JW, Oosterwijk C, Nieuwenhuis MG, Posthuma G, Thijssen JH, Vroom TM, Ahren B, Lips CJ: Extensive islet amyloid formation is induced by development of Type II diabetes mellitus and contributes to its progression: pathogenesis of diabetes in a mouse model. *Diabetologia* 42:427-434, 1999
24. Nevins AK, Thurmond DC: Glucose regulates the cortical actin network through modulation of Cdc42 cycling to stimulate insulin secretion. *Am J Physiol Cell Physiol* 285:C698-710, 2003
25. Tomas A, Yermen B, Min L, Pessin JE, Halban PA: Regulation of pancreatic beta-cell insulin secretion by actin cytoskeleton remodelling: role of gelsolin and cooperation with the MAPK signalling pathway. *J Cell Sci* 119:2156-2167, 2006
26. Howell SL, Tyhurst M: Interaction between insulin-storage granules and F-actin in vitro. *Biochem J* 178:367-371, 1979
27. Zheng W, Kollmeyer J, Symolon H, Momin A, Munter E, Wang E, Kelly S, Allegood JC, Liu Y, Peng Q, Ramaraju H, Sullards MC, Cabot M, Merrill AH, Jr.: Ceramides and other bioactive sphingolipid backbones in health and disease: lipidomic analysis, metabolism and roles in membrane structure, dynamics, signaling and autophagy. *Biochim Biophys Acta* 1758:1864-1884, 2006
28. Sjoholm A: Ceramide inhibits pancreatic beta-cell insulin production and mitogenesis and mimics the actions of interleukin-1 beta. *FEBS Lett* 367:283-286, 1995
29. Kelpe CL, Moore PC, Parazzoli SD, Wicksteed B, Rhodes CJ, Poitout V: Palmitate inhibition of insulin gene expression is mediated at the transcriptional level via ceramide synthesis. *J Biol Chem* 278:30015-30021, 2003
30. Lang F, Ullrich S, Gulbins E: Ceramide formation as a target in beta-cell survival and function. *Expert Opin Ther Targets* 15:1061-1071, 2011
31. Veret J, Coant N, Berdyshev EV, Skobeleva A, Therville N, Bailbe D, Gorshkova I, Natarajan V, Portha B, Le Stunff H: Ceramide synthase 4 and de novo production of ceramides with specific N-acyl chain lengths are involved in glucolipotoxicity-induced apoptosis of INS-1 beta-cells. *Biochem J* 438:177-189, 2011

32. Michaloglou C, Vredeveld LC, Soengas MS, Denoyelle C, Kuilman T, van der Horst CM, Majoor DM, Shay JW, Mooi WJ, Peeper DS: BRAFE600-associated senescence-like cell cycle arrest of human naevi. *Nature* 436:720-724, 2005
33. Braig M, Lee S, Loddenkemper C, Rudolph C, Peters AH, Schlegelberger B, Stein H, Dorken B, Jenuwein T, Schmitt CA: Oncogene-induced senescence as an initial barrier in lymphoma development. *Nature* 436:660-665, 2005
34. Collado M, Serrano M: Senescence in tumours: evidence from mice and humans. *Nat Rev Cancer* 10:51-57, 2010
35. Ruvolo PP: Intracellular signal transduction pathways activated by ceramide and its metabolites. *Pharmacol Res* 47:383-392, 2003
36. Spallarossa P, Altieri P, Barisione C, Passalacqua M, Aloi C, Fugazza G, Frassoni F, Podesta M, Canepa M, Ghigliotti G, Brunelli C: p38 MAPK and JNK antagonistically control senescence and cytoplasmic p16INK4A expression in doxorubicin-treated endothelial progenitor cells. *PLoS One* 5:e15583, 2010
37. Lupi R, Dotta F, Marselli L, Del Guerra S, Masini M, Santangelo C, Patane G, Boggi U, Piro S, Anello M, Bergamini E, Mosca F, Di Mario U, Del Prato S, Marchetti P: Prolonged exposure to free fatty acids has cytostatic and pro-apoptotic effects on human pancreatic islets: evidence that beta-cell death is caspase mediated, partially dependent on ceramide pathway, and Bcl-2 regulated. *Diabetes* 51:1437-1442, 2002
38. Baldwin AC, Green CD, Olson LK, Moxley MA, Corbett JA: A role for aberrant protein palmitoylation in FFA-induced ER stress and beta-cell death. *Am J Physiol Endocrinol Metab* 302:E1390-1398, 2012
39. Butler AE, Janson J, Bonner-Weir S, Ritzel R, Rizza RA, Butler PC: Beta-cell deficit and increased beta-cell apoptosis in humans with type 2 diabetes. *Diabetes* 52:102-110, 2003

Figure legends

Figure 1. Deoxysphingolipids decrease the replication of Ins-1 cells. A. Metabolic activity tested by MTT assay of Ins-1 cells treated at 50% (low density, L) and 90% (high density, H) confluence with sphinganine (SA) and 1-deoxysphinganine (dSA) at the indicated concentrations and incubated for 24 h. B. Enumeration of live cells treated with the indicated dSA concentrations for 24 h. Note that the number of cells treated with 1 μM dSA is comparable to the initial seeding density. C. Bright field images showing cell rounding up upon 24 h dSA treatment. D. Quantification of trypan blue positive cells after treatment with the indicated concentrations of dSA for 24 h. Data are expressed as percentage of total cell number. E. Quantification of LDH released in the medium after 24 h dSA treatment. Data are normalized to the number of cells. F. MTT assay of Ins-1cells treated with dSA for the indicated time and assessed 24 h after adding the lipid. Results are average ± SEM (n=3), *$p<0.05$. Scale bars: 50 μm.

Figure 2. 1-deoxysphinganine triggers senescence in Ins-1 cells. A. Quantification of β-galactosidase activity following incubation for 24 h with 1 μM sphinganine (SA), 0.5 and 1 μM 1-deoxysphinganine (dSA), or BSA as control (cntl). Values are normalized to the number of live cells. B. Immunofluorescence imaging showing nuclear expression of p21 following incubation for 24 h with 1 μM SA, 1 μM dSA, or BSA as control (cntl). Nuclei are stained with DAPI (blue). Lower panels show nuclear localization of p21. C. Western blot and densitometric quantification of p21/GAPDH levels following incubation for 24 h with 1 μM SA, 1 μM dSA or BSA as control. D. Immunostaining of p21 (upper panels) or live imaging (lower panel) of Ins-1 cells infected with p21 (Adp21) and GFP (AdGFP) adenoviruses at multiplicity of infection

(MOI) of 50. E. Enumeration of live Ins-1 cells 24 h after Adp21 or AdGFP infection. Note how Adp21 decreased the replication of Ins-1 cells in a dose response manner without inducing cell death. F. Quantification of β-galactosidase activity 24 h after Adp21 or AdGFP infection. Note how senescence is induced only in presence of Adp21. Results are average ± SEM (n=3), *p<0.05. Scale bars: 50 μm.

Figure 3. 1-deoxysphinganine triggers apoptosis and necrosis in Ins-1 cells. A. Left panel. Quantification of cleaved caspase 3 (CC-3) and p21 positive cells after 24 h incubation with 5 μM sphinganine, 1 and 5 μM 1-deoxysphinganine (dSA) or BSA as control. Right panel. Immunofluorescence imaging showing cytosolic expression of cleaved caspase 3 (CC-3). Note the pyknotic nuclei in CC-3 positive cells (arrows). Nuclei are stained with DAPI (blue). Results are average ± SEM (n=3), *p<0.05. Scale bars: 50 μm. B. FACS analyses of Ins-1 cells after 24 h incubation with 1 and 5 μM dSA or BSA as control and staining with PI and annexin V. C. Quantification of cells PI/ annexin V negative (live cells), PI positive (necrotic cells), annexin V positive (apoptotic cells) and double positive. Total population consisted of 20'000 cells. Note the increased lethality of cells treated with 5 μM 1-dSA.

Figure 4. 1-deoxy-dihydroceramide contributes to 1-deoxysphinganine-induced cytotoxicity in Ins-1 cells. A. MTT assay of Ins-1cells incubated for 72 h with sphinganine (SA), sphingosine (SO), 1-deoxysphinganine (dSA), deoxy-methylsphinganine (dmethSA), deoxy-dihydroceramides (1-deoxy-dh-Cer m18:0,24:1 and m18:0,16:0). B. Mass spectrometry quantification shows the increased formation of 1-deoxy-dh-Cer with different acyl chain length upon 24 h treatment with 3 μM 1 dSA. SA, SO and BSA incubation were used as control. C. RNA expression levels of different ceramide synthase (CerS) isoforms following lipid incubation as in B. Transcript levels were normalized using GAPDH RNA as a reference. D. Enumeration

of live cells following incubation for 24 h with dSA in presence or absence of 5 μM U-18666A or 35 μM fumonisin B1 (FB1). Results are average ± SEM (n=3), *p<0.05.

Figure 5. 1-deoxysphinganine increases the phosphorylation of selected kinases in Ins-1 cells. A. Western blot of phosphorylated and total levels of JNK, p38 and AKT following incubation for 24 h with 1 μM sphinganine (SA), 1 μM 1-deoxysphinganine (dSA) or BSA as control. B. Densitometric quantification of protein phosphorylation/total protein/actin levels. Data are expressed as percentage of control (cntl). C. Densitometric quantification of total protein/actin levels. Data are expressed as percentage of control (cntl). D. Enumeration of live cells treated with the indicated dSA concentrations for 24 h in presence of 10 μM of inhibitors of p38 MAPK (Birb796, Birb), JNK (SP600125, SP) or a combination of Birb796 and SP600125 (B/SP). Cells were pre-treated for 1 hour with the indicated inhibitors before addition of 1-deoxySA. E. Quantification of β-galactosidase activity following incubation for 24 h with 1 μM dSA in presence of 10 μM of inhibitors of p38 MAPK (Birb796, Birb), JNK (SP600125, SP) or a combination of Birb796 and SP600125 (B/SP). Values are normalized to the number of live cells. Results are average ± SEM (n=3), *p<0.05.

Figure 6. 1-deoxysphinganine incubation induced actin cytoskeleton rearrangements. A. Ins-1 cells treated with 5 μM 1-deoxysphinganine (dSA), sphinganine (SA) or BSA as control for 5 h and stained with phalloidin (green, left panels) or anti-tubulin antibody (red, right panels). Nuclei are stained with DAPI (blue). Note the actin staining in punctated structures following dSA treatment (arrows in left panel). In the right panels, arrows indicate tubulin midbody in recently divided cells and arrowhead the mitotic spindle. Scale bars: 50 μm. B. Rac1 activity following 5 h treatment with 5 μM dSA, 5 μM SA or BSA as control. NC, negative control. Constitutively active Rac1 (RCCA) was used as a positive control. C. Western blotting quantification of Rac1

and RhoA expression upon 24 h treatment with 1 μM dSA, 1 μM SA or BSA as control. Results are average ± SEM (n=3), *p<0.05. D. Confocal images of Ins-1 cells treated with 5 μM dSA or BSA as a control for 5 h and stained with phalloidin (green) or anti-insulin antibody (red). Nuclei are stained with DAPI (blue). Signal intensities representing the voxel space of the reconstructed image stacks are depicted as scatterplots showing partial signal overlap of actin and insulin in cntl and dSA-treated samples. Robust overlap of actin and β-catenin signals (dots accumulated in the mid-diagonal of the plot) and limited overlap of actin and DAPI (dots preferentially distributed along the axes) were used as a control. Nuclei are stained with DAPI (blue). Scale bars: 10 μm.

Figure 7. 1-deoxysphinganine treatment is cytotoxic for rat primary islets. Dissociated islets were plated on ECM plates and treated for 24 h with 5 μM sphinganine (SA), 5 μM 1-deoxysphinganine (dSA), and BSA as control. A. Quantification of vacuolized cells following lipid treatment. Data are expressed as percentage of total cell number. Right panels: bright field images of treated cells showing cell vacuolization (arrows and inset) upon dSA treatment. B. Metabolic activity tested by MTT assay. Data are expressed as percentage of BSA-treated control cells. C. Enumeration of live cells following lipid treatment. D. Quantification of insulin secretion stimulated with 3.3 mM (Low I), 16.7 mM (High) and 3.3 mM (Low II) glucose following incubation for 24 h with the lipids. Secreted insulin was normalized to the cell number. E. Filamentous actin (phalloidin, green) and insulin (red) co-staining of treated islets. Nuclei are stained with DAPI (blue). Results are average ± SEM (n=3), *p<0.05. Scale bars: 50 μm.

Figure 8. A. Mass spectrometry quantification of 1-deoxysphinganine (dSA) serum levels of 60 week old wild type (WT) and ob/ob mice. Results are average ± SEM (n=5), *p<0.05. B. Enumeration of live Ins-1 cells treated with the indicated dSA concentrations for 24 h in presence (Gluc) or absence (Cntl) of 30 mM glucose. Results are average ± SEM (n=3), *p<0.05.

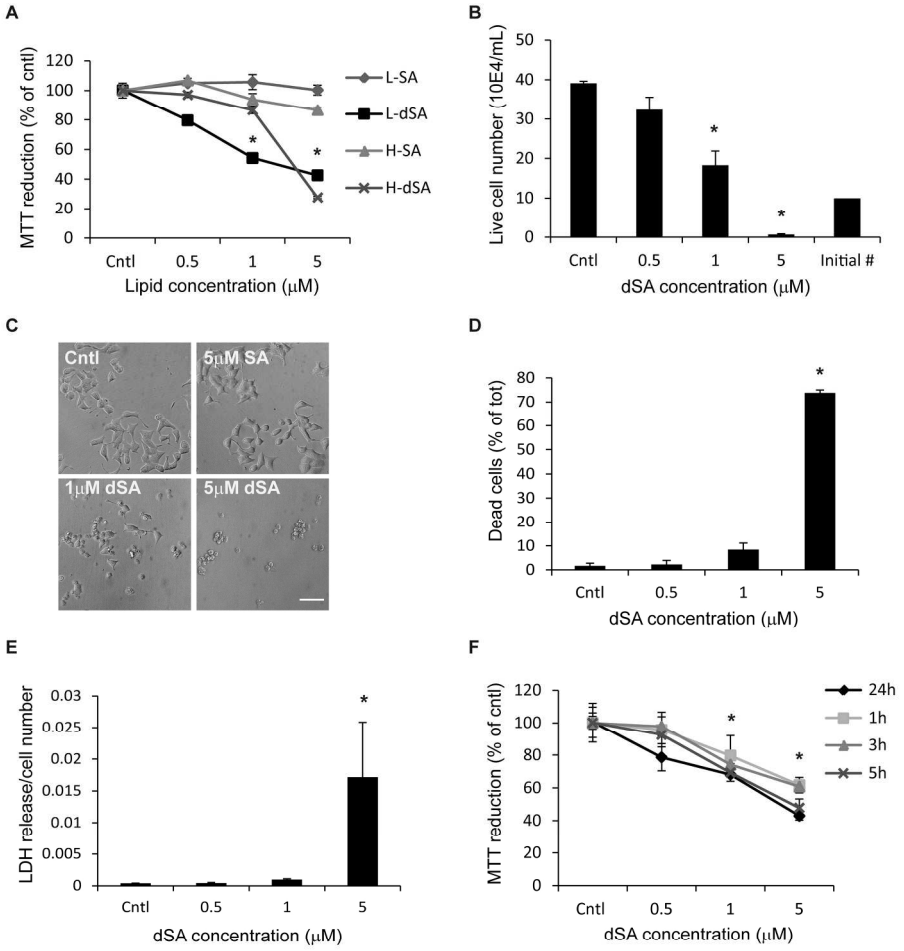

Fig. 1

203x211mm (300 x 300 DPI)

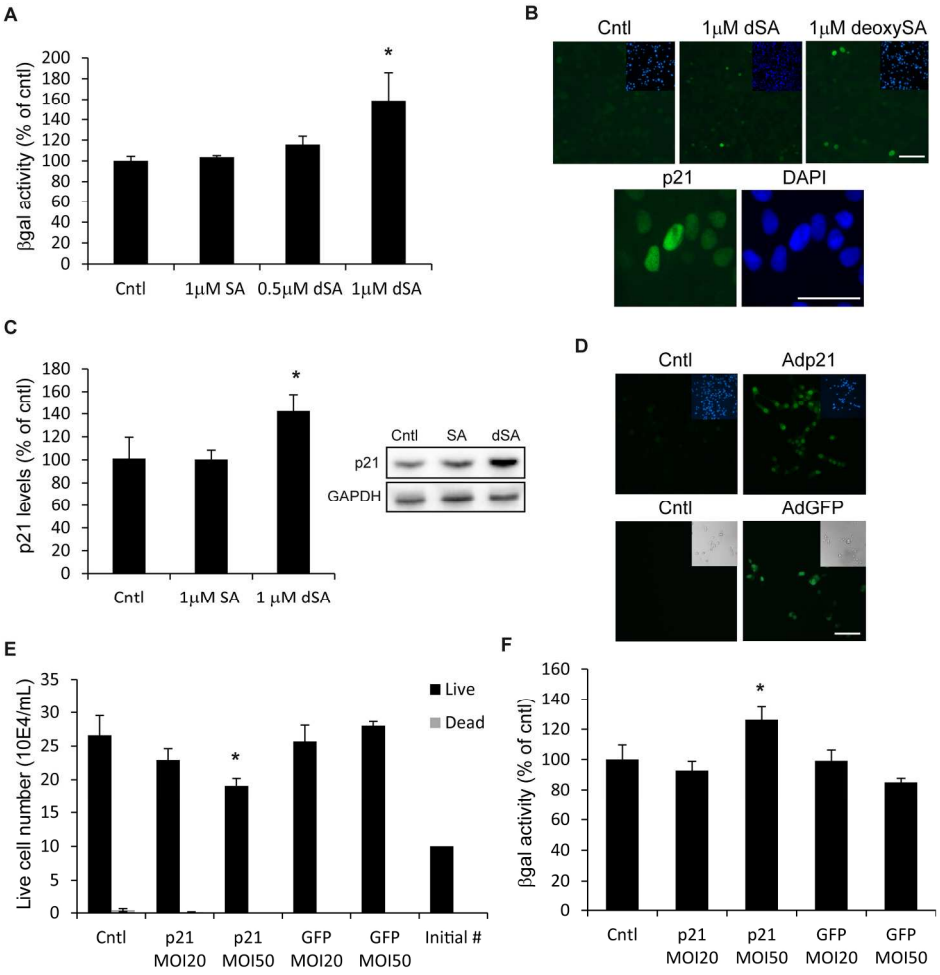

Fig. 2

203x222mm (300 x 300 DPI)

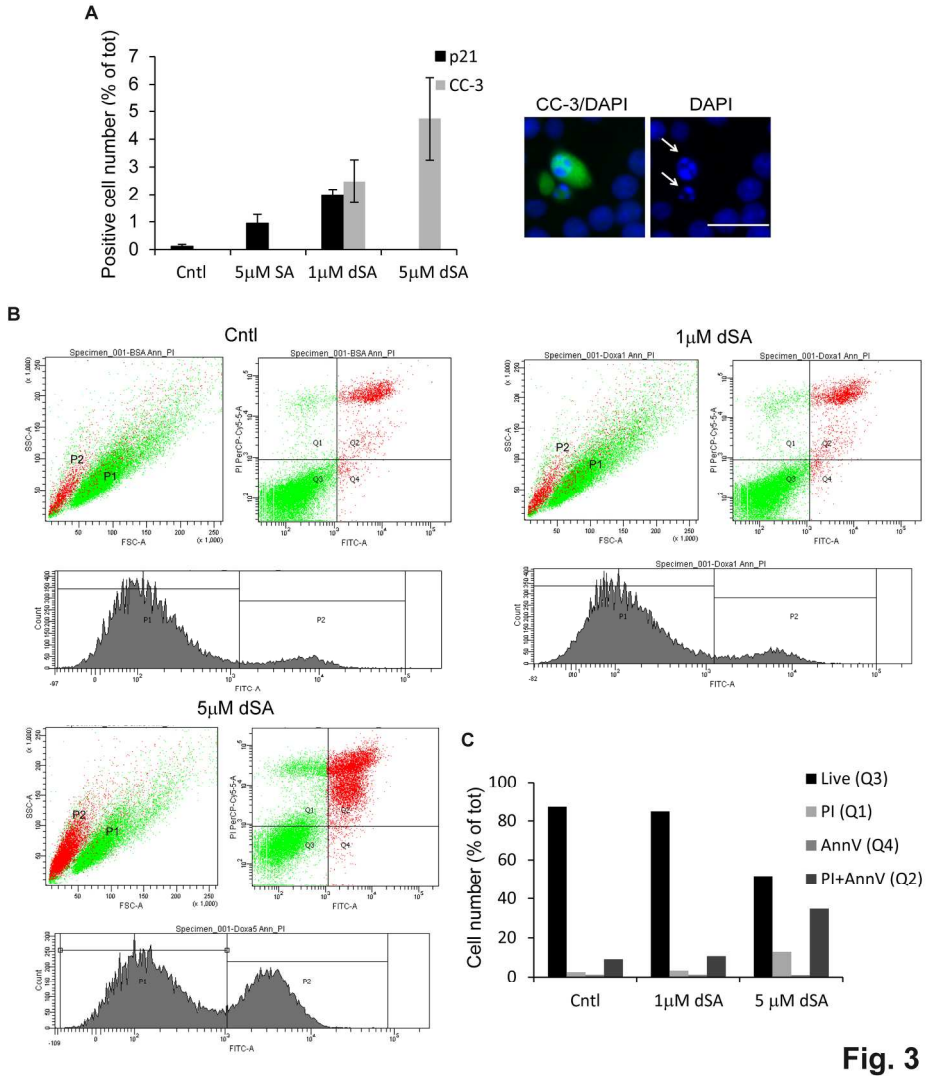

Fig. 3

203x218mm (300 x 300 DPI)

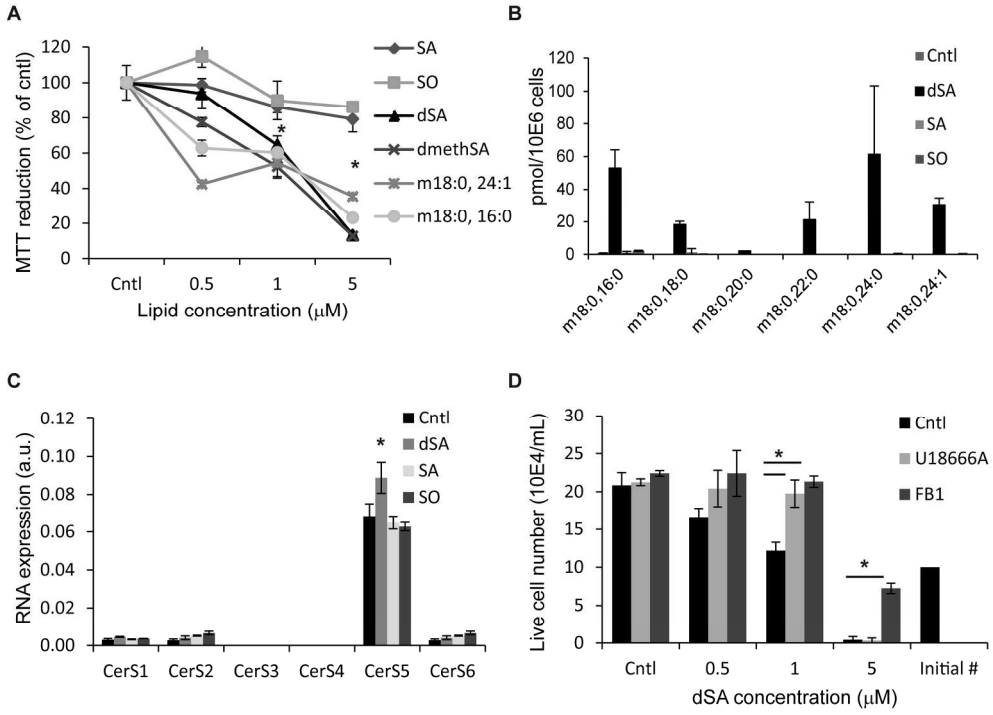

Fig. 4

204x231mm (300 x 300 DPI)

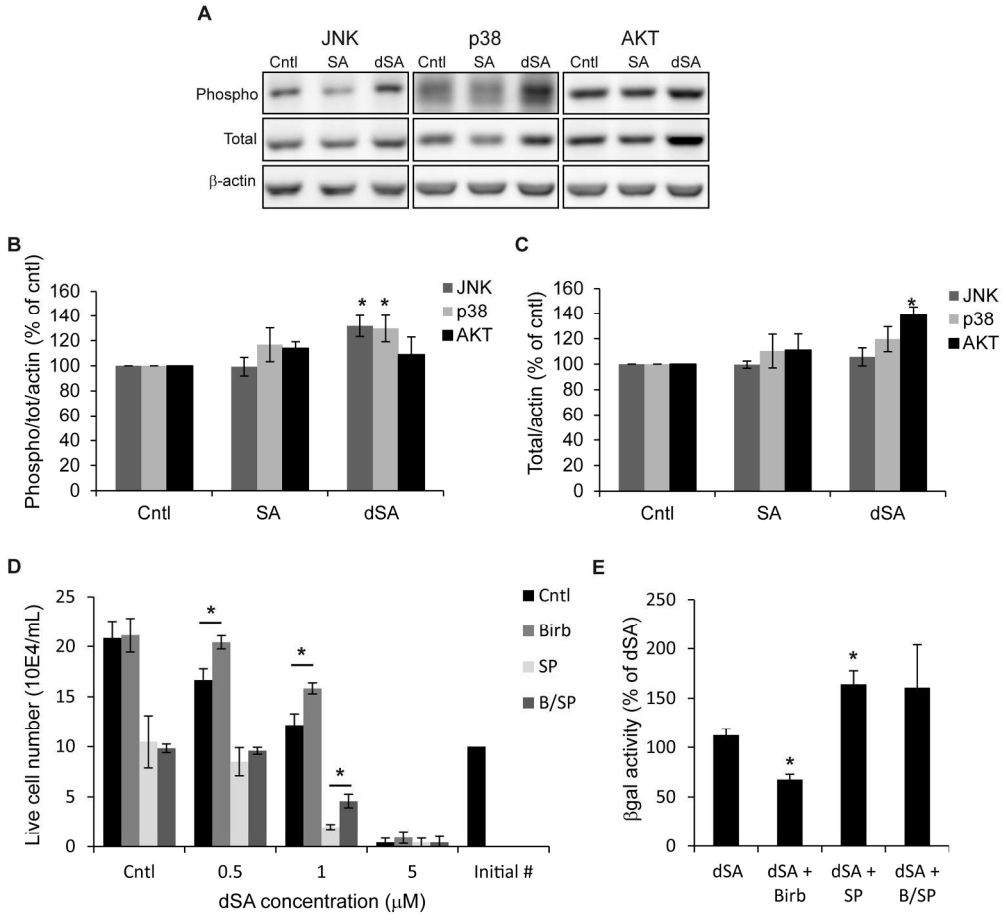

Fig. 5

203x231mm (300 x 300 DPI)

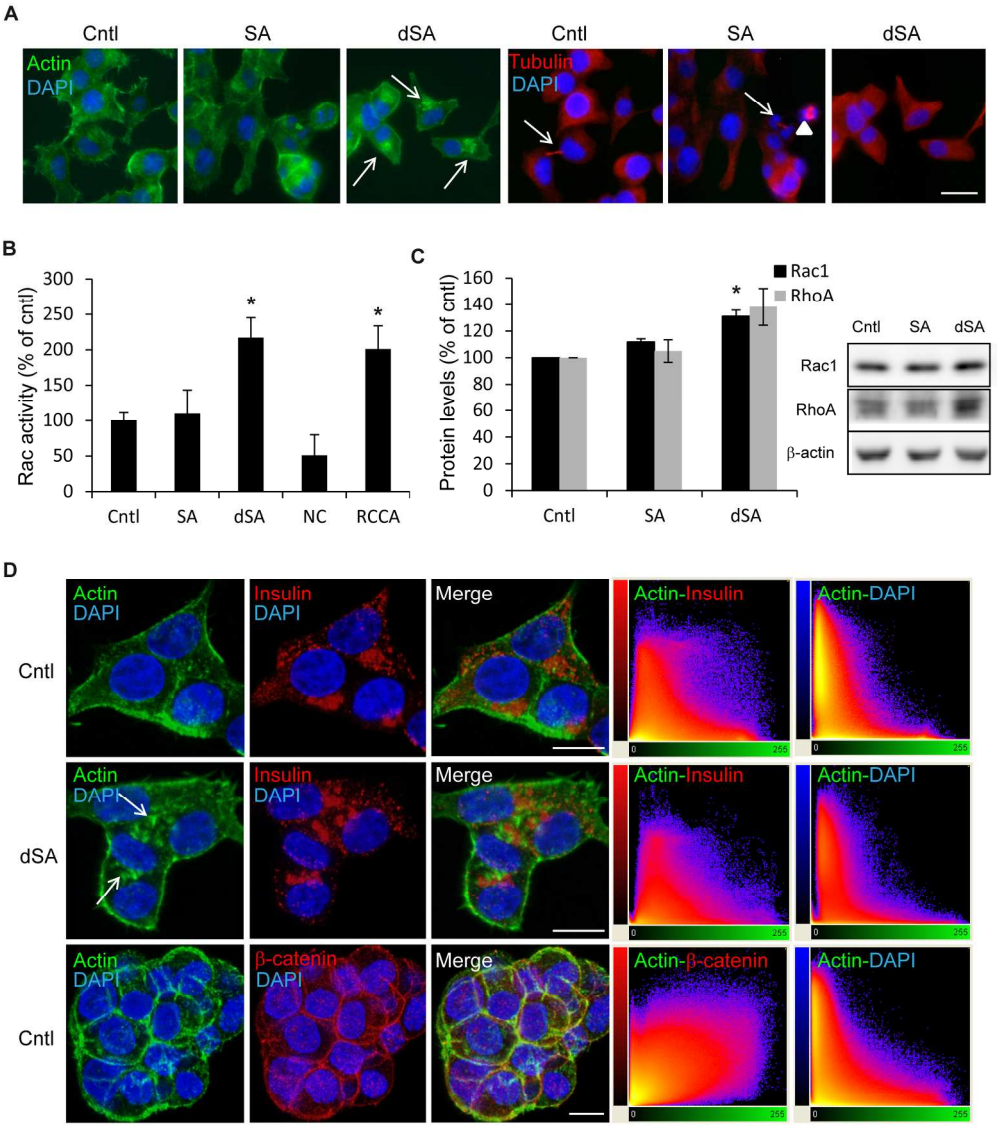

Fig. 6

208x246mm (300 x 300 DPI)

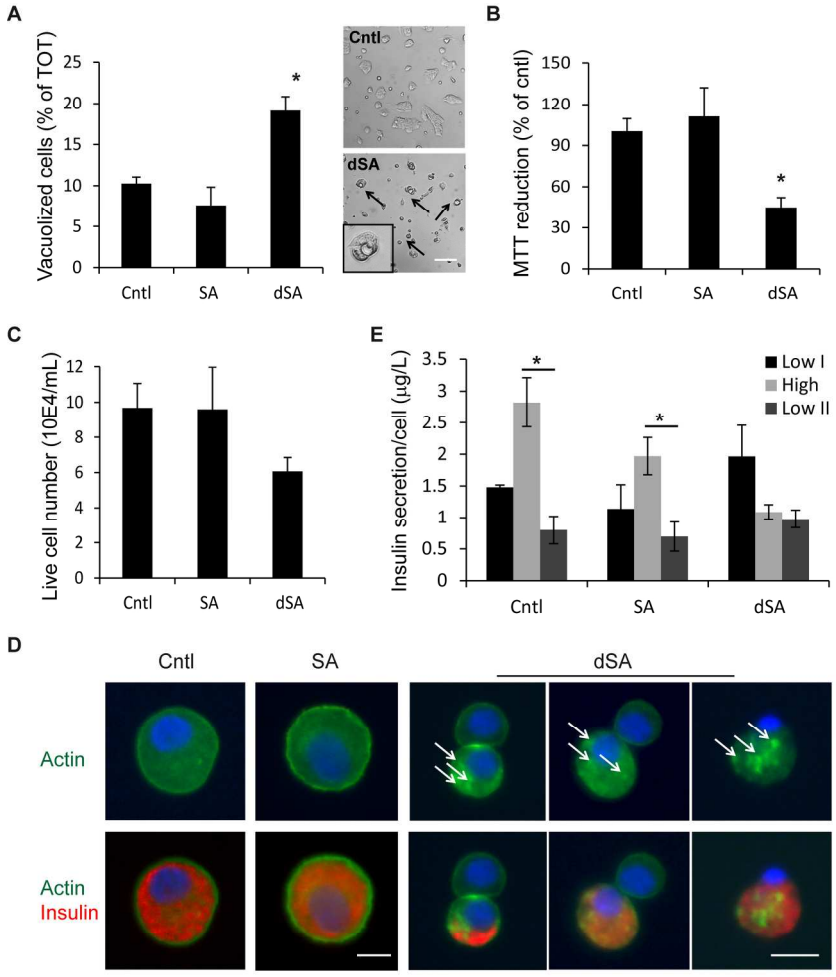

Fig. 7

197x223mm (300 x 300 DPI)

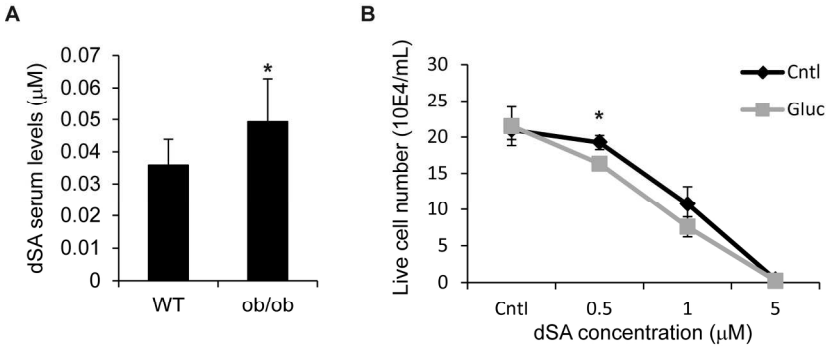

Fig. 8

201x240mm (300 x 300 DPI)

Supplementary Online Material

List of antibodies

Primary antibodies used for immunostaining were: Alexa Fluor 594 phalloidin (Life Technologies), anti-α–tubulin (Cell Signaling), anti-Rac1 (Abcam), anti-cleaved caspase-3 (Cell Signaling), anti-p21 (Abcam), anti-insulin (Dako), anti-glucagon (Sigma), fluorescein-conjugated Annexin V (BD Pharmingen). Fluorophore-conjugated secondary antibodies were from Alexafluor. Nuclei were visualized with 4′, 6-diamidino-2-phenylindole (DAPI).

Primary antibodies used for western blotting were: anti-p21 (Abcam), anti-GAPDH (Santa Cruz), anti-RhoA (Santa Cruz), anti-Rac1 (BD Biosciences), anti-phospho JNK and anti-JNK (R&D System), anti-phospho p38MAPK and anti-p38MAPK, anti-phospho AKT and anti-AKT (all from Cell Signaling) and anti-β-actin (Sigma). Secondary HRP-conjugated antibodies were from Jackson ImmunoResearch.

Ceramide synthase primers for qPCR

Rat CerS1: rat CerS1_LC_F: AGTGCCTGGAAGCTTCTGTT,

rat CerS1_LC_R: GACCTCCAGCCGTAGAAGAC

Rat CerS2: rat CerS2_LC_F: TTGAGGAAAGTTTGGGAAGG,

rat CerS2_LC_R: AAACCAGGAGAAGCAGAGGA

Rat CerS3: rat CerS3_LC_F: TGCCACACCTCTAGCCAATG,

rat CerS3_LC_R: CCTGGCGCTCTGTCAAGTTA

Rat CerS4: rat CerS4_LC_F: TCACTCTGCCCTTTGACATC,

rat CerS4_LC_R: TGACGCTGTAGGAGAAGACG

Rat CerS5: rat CerS5_LC_F: CACACAGCTGGCCTTCTACT,

rat CerS5_LC_R: ACTCGCACCATGTTGTTGAT

Rat CerS6: CerS6_F: GGGATCTTAGCCTGGTTCTGG,

CerS6_R: GCCTCCTCCGTGTTCTTCAG

Rat(Mouse)GAPDH: rat GAPDH_LC_F: GGTCGGTGTGAACGGATTTG,

rat GAPDH_LC_R: TTGCCGTGGGTAGAGTCATA

Figure legends

Figure S1. A. Comparison of Ins-1 metabolic activity by MTT and WST-1 reduction following 24 h incubation with 1-deoxysphinganine (dSA) at the indicated concentrations. BSA incubation was used as a control. Results are average ± SEM (n=3). B. Expression profile of genes involved in different cell death pathways following 1 μM dSA compared to 1 μM sphinganine incubation by Rat Cell Death Pathway Finder PCR Array (SABiosciences). 1 μM 1-deoxysphinganine treatment moderately up-regulated genes involved in necrosis, autophagy and apoptosis (Olr1583, Ctss, Esr1, Casp1, Fas), while anti-apoptotic genes (Bcl2a1d, Tnfrsf11b) were down-regulated. C. Analysis of extracted RNA integrity by Agilent 2100 Bioanalyzer. Examples of electrophoresis runs and assigned RNA integrity number (RIN) are shown. D. List of genes present in the array.

Figure S2. Analysis of MTT reduction /cell number following 24 h of 1-deoxysphinganine (dSA) treatment (A) or Adp21 and AdGFP infection (B). Data are expressed as percentage of control. Results are average ± SEM (n=5), *$p<0.05$.

Figure S3. 1-deoxysphinganine triggers apoptosis in Ins-1 cells. A. Co-staining with cleaved caspase 3 (CC-3, red) and p21 (green) showing the mutually exclusive expression of the proteins upon incubation for 24 h with 5 μM sphinganine, 1 and 5 μM 1-deoxysphinganine or BSA as control. Nuclei are stained with DAPI (blue). Scale bars: 50 μm. B. FACS based quantification of

dead cells following 24 h incubation with 1 and 5 μM dSA or BSA as control as determined by FSC and SSC parameters shown in Fig. 3.

Figure S4. Cell cycle analysis by quantification of DNA content in Ins-1 cells after 24 h incubation with 1 and 5 μM 1-deoxysphinganine (dSA) or BSA as control. The amount of cells in different cell cycle phases is plotted in the lower panel. Total population consisted of 20'000 cells. Note the decreased amount of cells in G2/M phase and accumulation in G0/G1 phase following 5 μM 1-deoxysphinganine treatment.

Figure S5. A. Mass spectrometry quantification of ceramides in Ins-1 cells treated for 24 h with 3 μM of sphinganine (SA), sphingosine (SO), 1-deoxysphinganine (dSA) and BSA as control. B. MTT assay following incubation for 24 h with SA or dSA in presence or absence of 5 μM U-18666A (U). C. Bright field images of Ins-1 cells showing reduced toxicity following 5 μM dSA treatment in presence of FB1. Results are average ± SEM (n=3), *$p<0.05$. Scale bars: 50 μm.

Figure S6. A. Ins-1 cells were treated with 10 μM of inhibitors of JNK (SP600125, SP), p38 MAPK (Birb796, Birb) or 35μM ceramide synthase inhibitor FB1 for 1 h, followed by 5 h treatment with 5 μM 1-deoxysphinganine (dSA), sphinganine (SA) or BSA and phalloidin staining. Nuclei are stained with DAPI (blue). Scale bars: 50 μm. B. FACS-based quantification of actin and insulin cellular content following 5 h treatment with 5 μM dSA, SA or BSA.

Figure S7. Dissociated islets were plated on ECM plates and treated for 24 h with 5 μM sphinganine (C18SA), 1-deoxysphinganine (dSA), and BSA as control. A. Quantification of β-galactosidase activity normalized by the cell number. B. Quantification of cellular insulin content. Cells were lysed and total insulin level was normalized by the cell number. C. Enumeration of insulin-expressing cells. Data are expressed as percentage of total cell number.

D. Quantification of insulin secretion stimulated with 3.3 mM (Low I), 16.7 mM (High) and 3.3 mM (Low II) glucose following incubation for 24 h with the lipids. Secreted insulin was normalized by the total insulin content. Results are average ± SEM (n=3), *p<0.05.

Figure S8. A. Weight and blood parameters of WT and ob/ob mice. B. Histological morphology (HE staining) of paraffin embedded liver and pancreas sections from WT and ob/ob mice. Note the accumulation of lipid deposit and steatotic phenotype in the latter. Staining of insulin/glucagon, replicating (Ki67), senescent (p21) and apoptotic cells (TUNEL) in islets of 60 week old wild type (WT) and ob/ob mice. Nuclei are stained with DAPI (blue). Scale bars: 50 μM. D. Mass spectrometry quantification of serum levels of total sphingoid bases after hydrolyzing the head group and N-linked fatty acid. Results are average ± SEM (n=5), *p<0.05. E. MTT assay of Ins-1 cells incubated for 24 h with 1-deoxysphinganine in presence (Gluc) or absence (Cntl) of 30 mM glucose. Results are average ± SEM (n=3), *p<0.05.

A

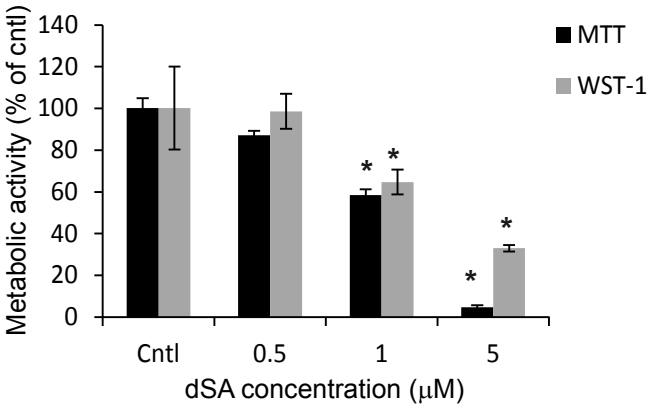

B

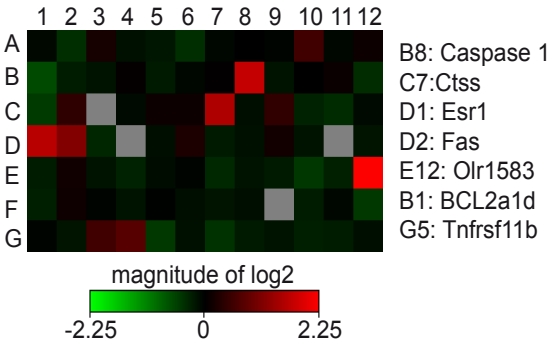

C

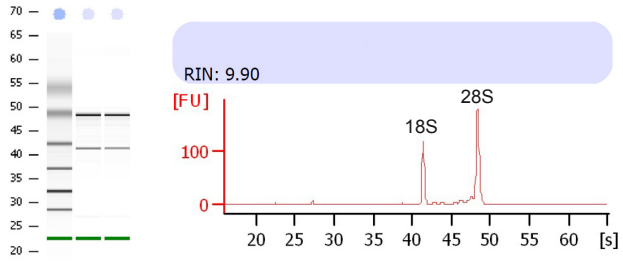

D

Well	Gene symbol
A01	Abl1
A02	Akt1
A03	Apaf1
A04	App
A05	Atg12
A06	Atg16l1
A07	Atg3
A08	Atg5
A09	Atg7
A10	Atp6v1g2
A11	Bax
A12	Bcl2
B01	Bcl2a1d
B02	Bcl2l1
B03	Bcl2l11
B04	Becn1
B05	Birc2
B06	Birc3
B07	Bmf
B08	Casp1
B09	Casp2
B10	Casp3
B11	Casp6
B12	Casp7
C01	Casp9
C02	Cd40
C03	Cd40lg
C04	Cflar
C05	Commd4
C06	Ctsb
C07	Ctss
C08	Cyld
C09	Defb1
C10	Dffa
C11	Dpysl4
C12	Eif5b
D01	Esr1
D02	Fas
D03	Faslg
D04	Foxi1
D05	Gaa
D06	Gadd45a
D07	Galnt5
D08	Grb2
D09	Hspbap1
D10	Htt
D11	Ifng
D12	Igf1

Well	Gene symbol
E01	Igf1r
E02	Ins2
E03	Irgm
E04	Jph3
E05	Kcnip1
E06	Mag
E07	Map1lc3a
E08	Mapk8
E09	Mcl1
E10	Nfkb1
E11	Nol3
E12	Olr1583
F01	Parp1
F02	Parp2
F03	Pik3c3
F04	Pvr
F05	Rab25
F06	RGD1311517
F07	RGD1562639
F08	Rps6kb1
F09	S100a7a
F10	Snca
F11	Spata2
F12	Sqstm1
G01	Sycp2
G02	Tmem57
G03	Tnf
G04	Tnfrsf10b
G05	Tnfrsf11b
G06	Tnfrsf1a
G07	Tp53
G08	Traf2
G09	Txnl4b
G10	Ulk1
G11	Uvrag
G12	Xiap
H01	Rplp1
H02	Hprt1
H03	Rpl13a
H04	Ldha
H05	Actb

Fig. S1

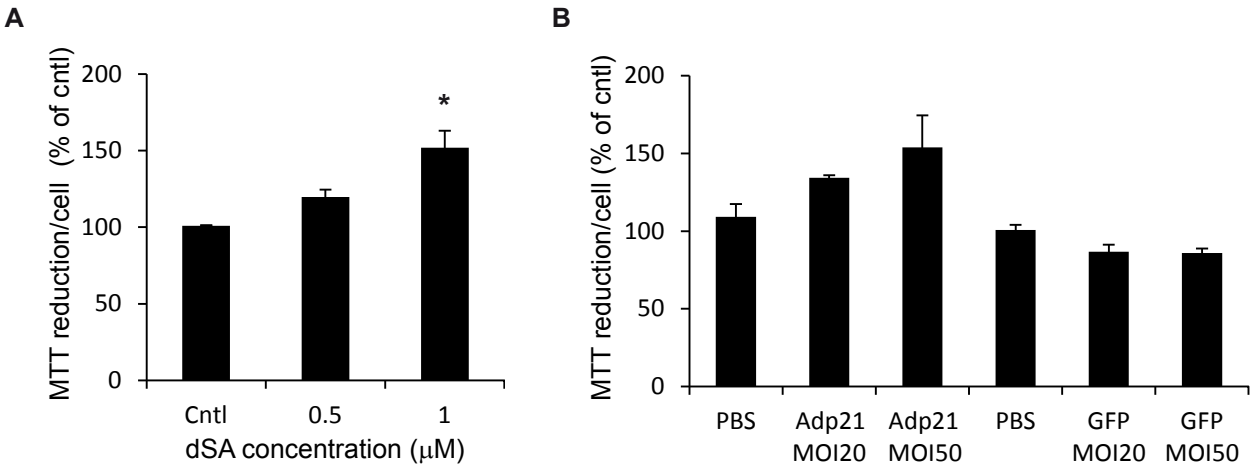
A
MTT reduction/cell (% of cntl)
200
150
100
50
0
*
Cntl
0.5
1
dSA concentration (μM)
B
MTT reduction/cell (% of cntl)
200
150
100
50
0
PBS
Adp21 MOI20
Adp21 MOI50
PBS
GFP MOI20
GFP MOI50

Fig. S2

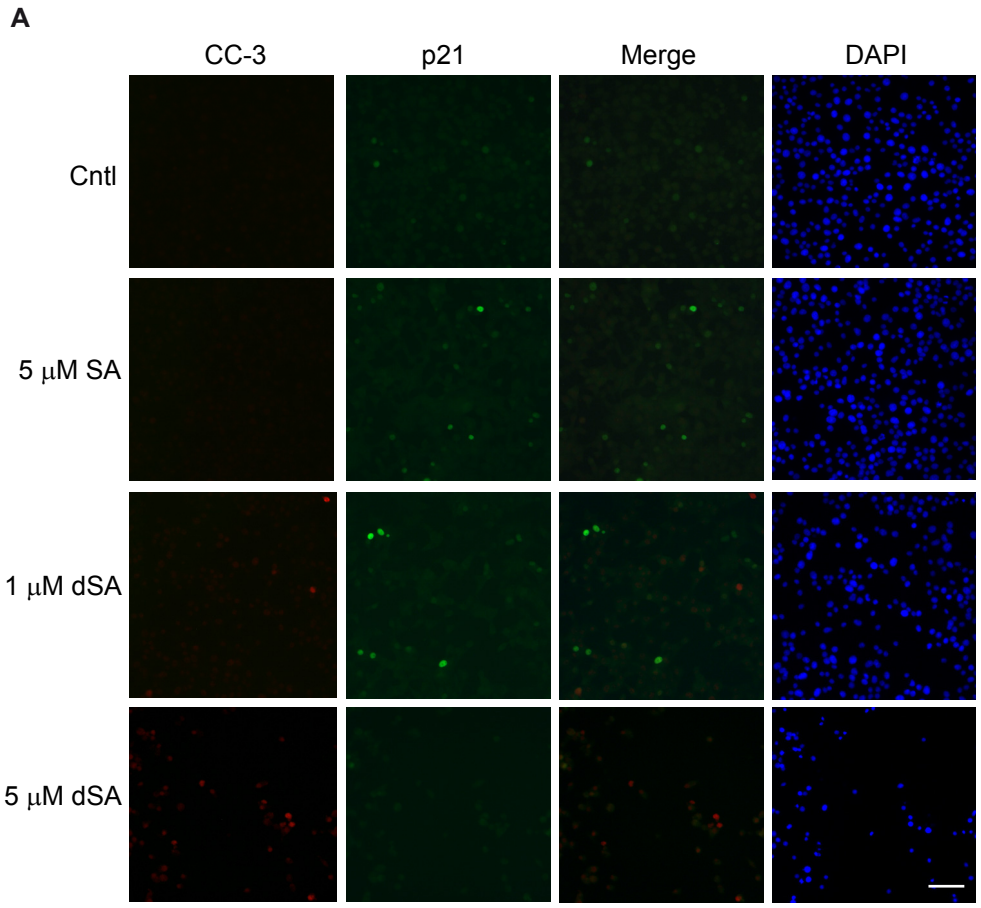
A
CC-3
p21
Merge
DAPI
Cntl
5 μM SA
1 μM dSA
5 μM dSA

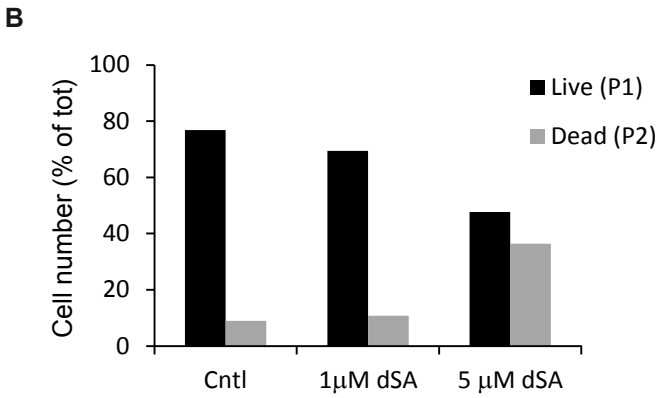
B
Cell number (% of tot)
100
80
60
40
20
0
Live (P1)
Dead (P2)
Cntl
1μM dSA
5 μM dSA

Fig. S3

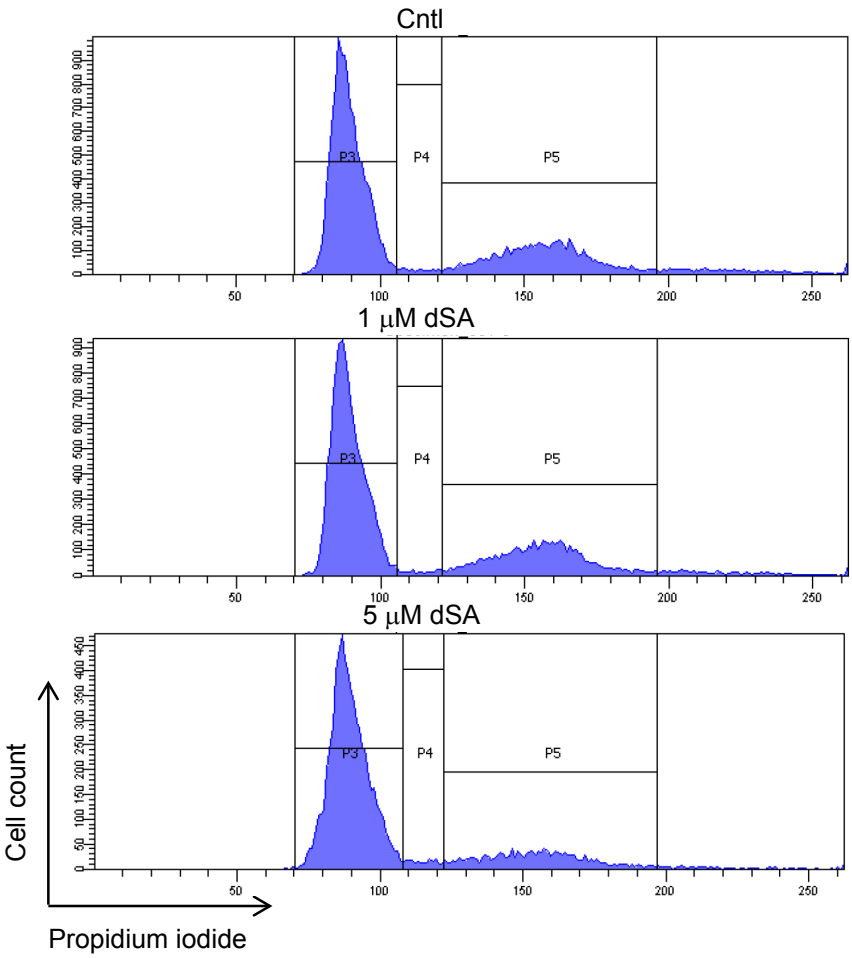
Cntl
P3
P4
P5
1 μM dSA
P3
P4
P5
5 μM dSA
P3
P4
P5
Cell count
Propidium iodide

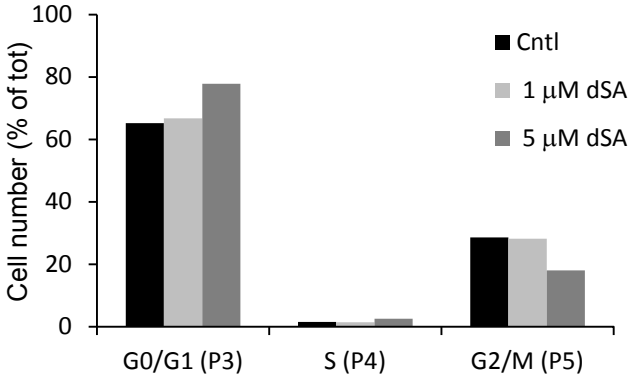
Cell number (% of tot)
100
80
60
40
20
0
Cntl
1 μM dSA
5 μM dSA
G0/G1 (P3)
S (P4)
G2/M (P5)

Fig. S4

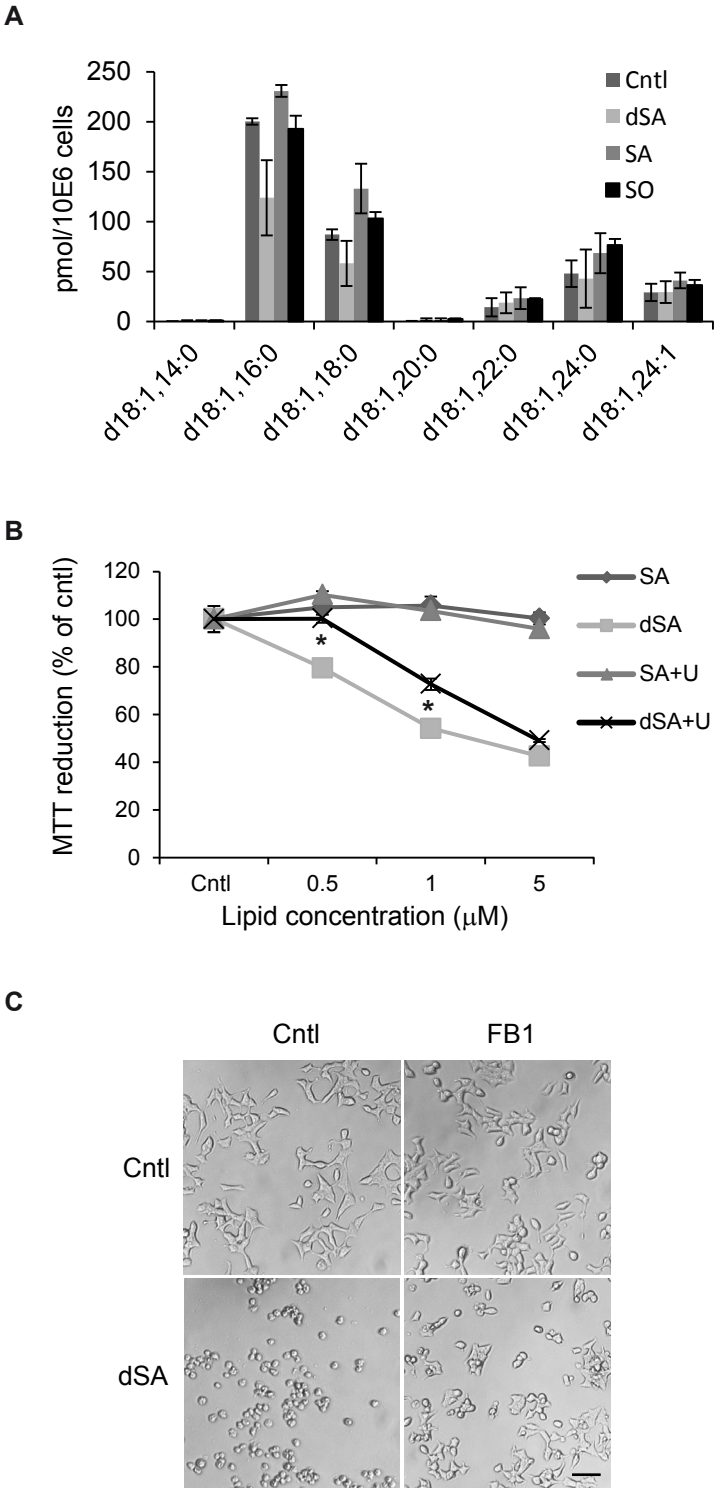
A
pmol/10E6 cells
250
200
150
100
50
0
Cntl
dSA
SA
SO
d18:1,14:0
d18:1,16:0
d18:1,18:0
d18:1,20:0
d18:1,22:0
d18:1,24:0
d18:1,24:1
B
MTT reduction (% of cntl)
120
100
80
60
40
20
0
SA
dSA
SA+U
dSA+U
Cntl
0.5
1
5
Lipid concentration (μM)
C
Cntl
FB1
Cntl
dSA

Fig. S5

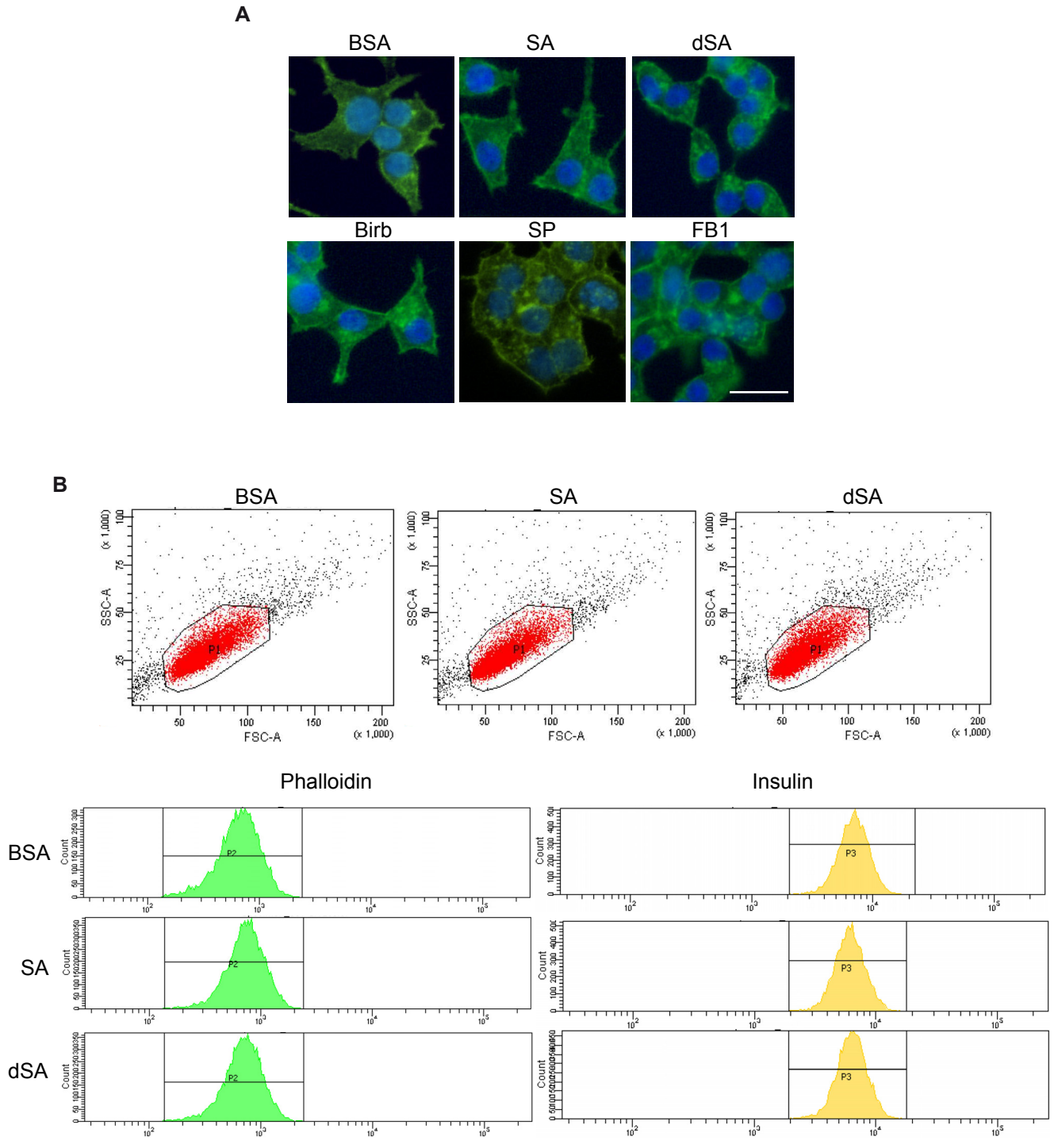
A
BSA
SA
dSA
Birb
SP
FB1
B
BSA
SA
dSA
SSC-A
FSC-A
(x 1,000)
P1
Phalloidin
Insulin
BSA
SA
dSA
Count
P2
P3

Fig. S6

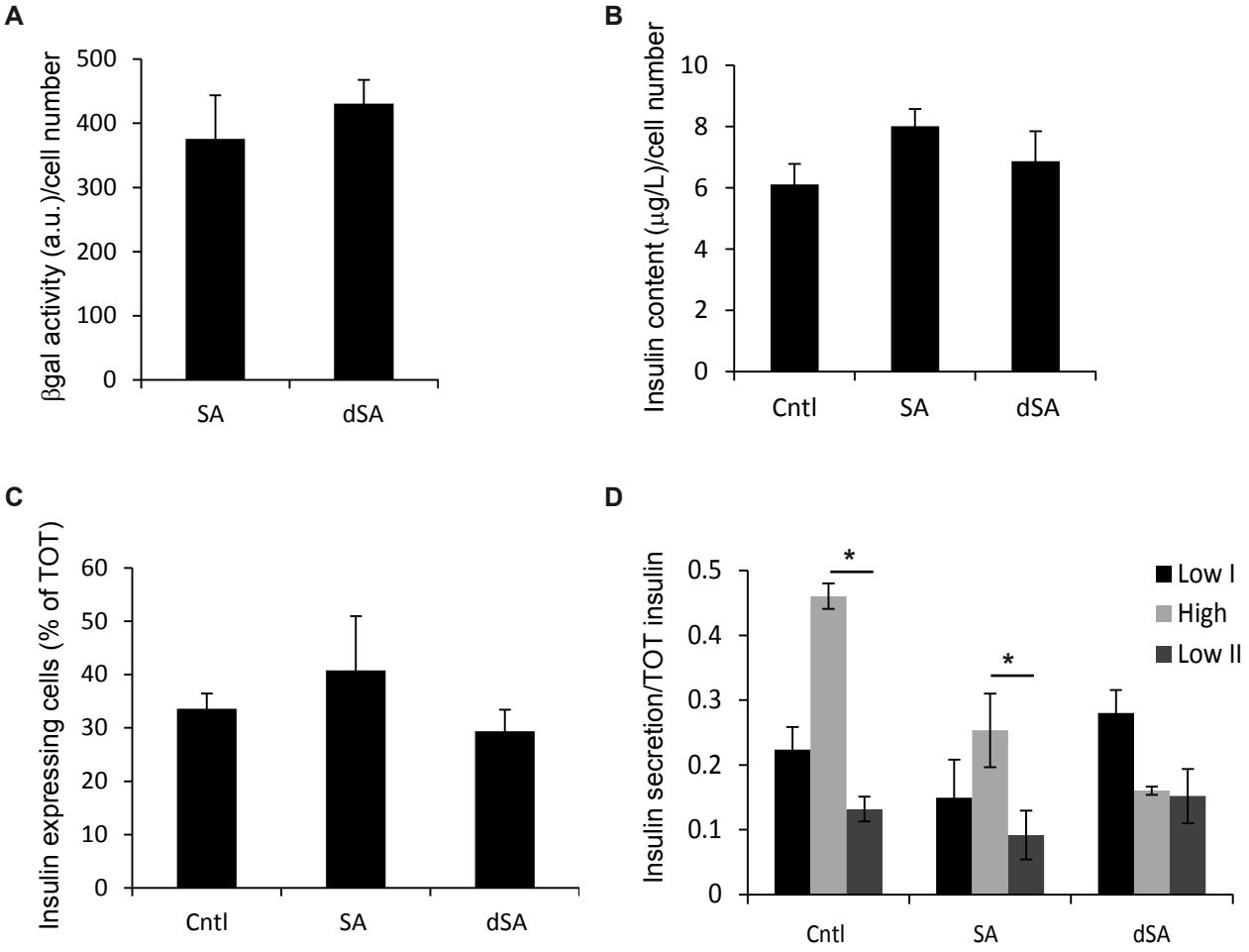
A
βgal activity (a.u.)/cell number
500
400
300
200
100
0
SA
dSA
B
Insulin content (μg/L)/cell number
10
8
6
4
2
0
Cntl
SA
dSA
C
Insulin expressing cells (% of TOT)
60
50
40
30
20
10
0
Cntl
SA
dSA
D
Insulin secretion/TOT insulin
0.5
0.4
0.3
0.2
0.1
0
*
*
Low I
High
Low II
Cntl
SA
dSA

Fig. S7

A

	Weight (G)	Glucose (mmol/L)	TG (mmol/L)	HDL (mmol/L)	Chol (mmol/L)	ALT (U/L)
WT	41.3+/-1.77	10.9+/-0.61	0.89+/-0.09	2.02+/-0.127	2.36+/-0.139	10.88+/-0.61
ob/ob	82.3+/-1.43	14.92+/-1.23	0.94+/-0.14	4.81+/-0.57	5.77+/-0.59	102.87+/-24.3
P value	3.01E-10	0.008098	0.765418	0.000128	2.83E-05	0.001008

TG, triacylglycerol; HDL, high density lipoprotein; Chol, cholesterol; ALT, alanine aminotransferase. Values are expressed as means ± SEM (N=7)

B

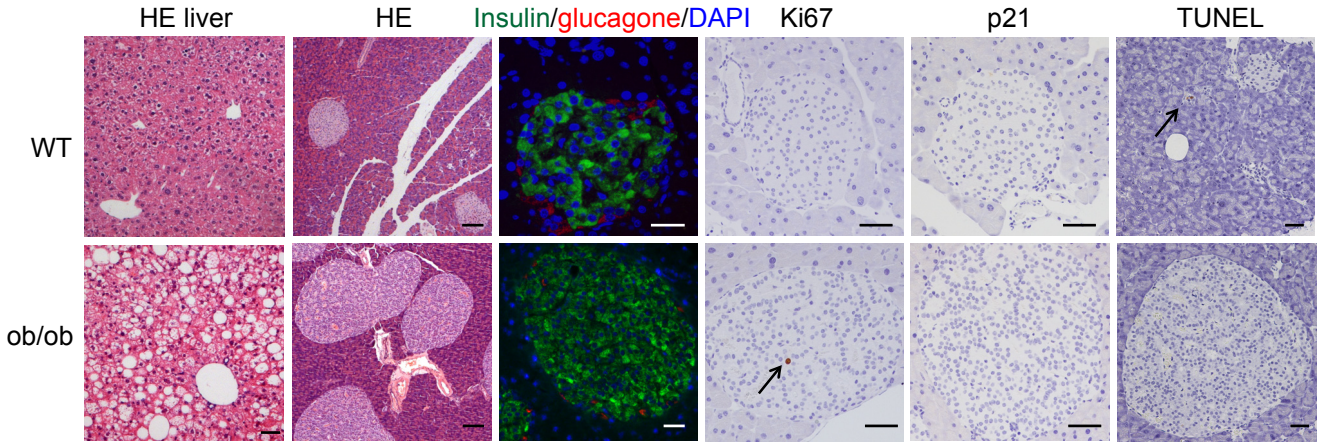

C

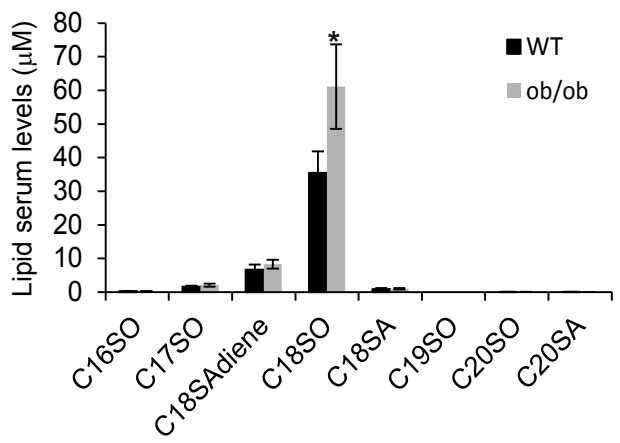

D

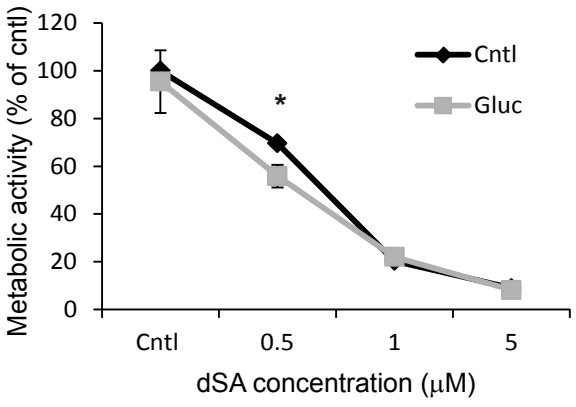

Fig. S8